A Method for On-line Water Current Velocity Estimation Using Low-cost Autonomous Underwater Vehicles

by
Lieutenant Commander Christopher R. Dolan, United States Navy
B.S., University of Washington, 2007
Submitted to the Joint Program in Applied Ocean Science & Engineering
in partial fulfillment of the requirements for the degree of
Master of Science in Mechanical Engineering
at the
MASSACHUSETTS INSTITUTE OF TECHNOLOGY
and the
WOODS HOLE OCEANOGRAPHIC INSTITUTION
September 2020

Author .....
Joint Program in Applied Ocean Science & Engineering
Massachusetts Institute of Technology
& Woods Hole Oceanographic Institution
August 09, 2020

Certified by .....
Michael Jakuba
Senior Engineer
Woods Hole Oceanographic Institution
Thesis Supervisor

Certified by .....
Erin M. Fischell
Assistant Scientist
Woods Hole Oceanographic Institution
Thesis Supervisor

Accepted by .....
Nicolas Hadjiconstantinou
Chairman, Mechanical Engineering Committee for Graduate Students
Massachusetts Institute of Technology

Accepted by .....
David K. Ralston
Chairman, Joint Committee for Applied Ocean Science & Engineering
Massachusetts Institute of Technology
Woods Hole Oceanographic Institution

A Method for On-line Water Current Velocity Estimation Using Low-cost Autonomous Underwater Vehicles

by

Lieutenant Commander Christopher R. Dolan, United States Navy

Submitted to the Joint Program in Applied Ocean Science & Engineering
Massachusetts Institute of Technology
& Woods Hole Oceanographic Institution
on August 09, 2020, in partial fulfillment of the
requirements for the degree of
Master of Science in Mechanical Engineering

Abstract

Advances in the miniaturization of microelectronics has greatly contributed to the proliferation of small, low cost autonomous underwater vehicles (AUVs). These affordable vehicles offer organizations a flexible platform that can be adapted to support a multitude of research goals. The small size and low entry cost come with a trade off of simple navigation systems, typically dead reckoning (DR) using a speed determined via propeller counts and heading from a low cost micro-electromechanical system (MEMS) inertial measurement unit (IMU), whose error grows unbounded without the availability of a ground referenced fix source and is compounded by the bias present in the speed measurement due to the change in hydrodynamics from the addition of sensors to the hull form. Additionally, some capabilities such as water current velocity measurement traditionally requires the addition of equipment that is not only expensive, but also whose size and power consumption can adversely affect operating characteristics and deployment times. This thesis expands on previous research using one-way travel time inverted USBL (OWTT-iUSBL) to calculate the local current velocity without the addition of a Doppler velocity log (DVL) or acoustic Doppler current profiler (ADCP). A novel extended Kalman filter (EKF) is proposed that, in addition to calculating the current velocity, estimates and corrects for the bias present in the speed measurement as determined by the main vehicle computer. Using data collected on the Charles River at the Massachusetts Institute of Technology (MIT) Sailing Pavilion, it is shown that current velocities can be reasonably calculated using OWTT-iUSBL data as compared to the values calculated using long baseline (LBL) data.

Thesis Supervisor: Michael Jakuba
Title: Senior Engineer
Woods Hole Oceanographic Institution

Thesis Supervisor: Erin M. Fischell
Title: Assistant Scientist
Woods Hole Oceanographic Institution

Acknowledgments

Funding for this thesis research was provided the US Navy Civilian Institutions Office through the Massachusetts Institute of Technology/Woods Hole Oceanographic Institution Joint Program.

Thank you to my wife Jabin for your patience and perseverance during this process. Your love and support are the anchor for our family when the seas get rough. For my young sons Carrick and Rhys, you may have been frustrated when I had to be gone all day commuting up to Boston or when I couldn't play even when I was home working, but thank you for being excited to spend time together when I was available.

Thank you to my research advisors, Dr. Michael Jakuba and Dr. Erin Fischell for your incredible support. Beginning with course scheduling, continuing through simulations and field work and culminating with thesis writing, your guidance and mentorship paved the way for the successful completion of my research.

Thank you to my academic advisor, Prof. Henrik Schmidt. Your assistance with both scheduling and class work was invaluable to setting the groundwork for my research.

Thank you to fellow members of the Marine Unmanned Robotics and Acoustics Lab, Dr. Nick Rypkema, Dr. Pedro Vaz Teixeira, Caileigh Fitzgerald and Kevin Manganini for your assistance in coding, fabrication and data collection in support of my thesis research.

Thank you to my fellow Navy Joint Program students Brendan O'Neill, Mike Humara and John Li for your friendship and collaboration throughout our journey.

Contents

List of Figures

List of Tables

List of Acronyms

ADCP	acoustic Doppler current profiler
AHRS	attitude and heading reference system
AUG	autonomous underwater glider
AUV	autonomous underwater vehicle
CMKF	converted measurements Kalman filter
CSAC	chip-scale atomic clock
DR	dead reckoning
DVL	Doppler velocity log
EKF	extended Kalman filter
GPS	global positioning system
IMU	inertial measurement unit
KF	Kalman filter
LBL	long baseline
MEMS	micro-electromechanical system
MIT	Massachusetts Institute of Technology
MMSE	minimum mean squared error
NaN	not-a-number
NCV	nearly constant velocity
NEES	normalized estimation error squared
NIS	normalized innovation squared

NMEE	normalized mean estimation error
OWTT-iUSBL	one-way travel time inverted USBL
RPM	revolutions per minute
USBL	ultra-short baseline

Chapter 1

Introduction

Autonomous underwater vehicles (AUVs) provide an ideal platform for many commercial, academic and military applications due to their small size, quiet operation and ability to operate without direct control. Such applications include underwater structure inspection, ocean floor mapping and surveillance. In order for AUVs to properly conduct their missions, they first must be able to localize themselves geographically. While surfaced, the global positioning system (GPS) provides satellite signal that translate into an average user range error of ≤ 7.8 m. Because electromagnetic radiation will not penetrate the water to a significant distance, GPS signals cannot be received while the AUV is submerged and other methods such as dead reckoning (DR), inertial or acoustic navigation must be used.

DR navigation uses the integration of the speed of the vehicle with time, usually determined as a function of propeller turn count or bottom track velocities from a Doppler velocity log (DVL), combined with the heading of the vehicle from a compass or an attitude and heading reference system (AHRS) to determine the change in geographical position. While relatively simple, DR navigation is subject to several significant sources of error. First, because the speed vs. turn count model is calibrated at the factory prior to delivery, any change to the hydrodynamic shape or displacement of the AUV will induce a bias into water referenced speed measurement. Additionally, the accuracy of instrument calibration and drift over time will induce biases in all measurements. Furthermore, the local current field exerts forces that are unaccounted by any instrument. These sources contribute to an error that grows unbounded with time.

Inertial navigation uses an inertial measurement unit (IMU) as part of an inertial nav-

igation system (INS) to measure vehicle acceleration in three axes and then perform two integration operations to determine the change in geographical position. While an IMU with physical dimensions compatible with AUV use exhibits less noise than a typical AHRS, the gyro bias and drift cause unbounded error growth on the order of 2-5% of the distance traveled. [9].

Acoustic navigation can be implemented in several forms. In a long baseline (LBL) scheme, multiple transducers are placed at a fixed geographic location to form an array. When the AUV sends a query signal to the transducers, each element of the array sends a response ping. With knowledge of the array configuration, time difference between pings and the local sound speed, the location of the AUV can be calculated accurately. With a typical 10 kHz LBL network, position accuracy can be as good as one to 10 m at ranges of up to 10 km [7].

Another configuration common to AUVs uses one transponder, usually on a surface vessel, and a multi-element transducer array on the AUV and is referred to as ultra-short baseline (USBL). When the AUV sends a query ping, the surface vessel transducer sends a response ping. Because the array on the AUV contains more than one element, the angles of azimuth and elevation to the surface transducer can be calculated. With these angles, the knowledge of the time of flight of the signal and the local sound speed, the position relative to the surface transponder can be calculated [7].

Another variant of USBL, the one-way travel time inverted USBL (OWTT-iUSBL) uses a surface transmitter and a multi-element receiving array on the AUV. Unlike a traditional USBL, the surface vessel transmits a signal at specified time intervals which are received and processed on the AUV. In order to properly calculate relative position, the AUV uses a precision timing source such as a chip-scale atomic clock (CSAC) which is synchronized to GPS prior to deployment and when surfacing for GPS measurements. This method reduces the power consumption of the AUV by eliminating the requirement to transmit to the surface vessel. Jakuba et al. [6] discussed the feasibility and additional advantages of this method which include improvement in navigational accuracy and increased data collection time by reducing the number of surfacing operations for GPS required to maintain an adequate navigational picture. Each of these methods has advantages and disadvantages, and in practice, multiple data streams are used as inputs to an algorithm which fuses the sources of information and seeks to produce the best available state estimate.

One common way to provide additional information to bound error growth for either DR or inertial navigation is to add a DVL. A DVL typically consists of an array of four or five transducer elements installed on the vehicle facing the sea floor. As long as the AUV is close enough to the sea floor to achieve bottom lock, the DVL calculates the vehicle's geographically referenced velocity, which can be fused with the DR or inertial navigation solution to provide a more constrained estimate of vehicle motion [7].

Another method to reduce the error associated with DR is to use a vehicle model which seeks to provide a more accurate estimation of vehicle motion than simply using the turn count. Hegrenæs and Hallingstad examined the effectiveness of using a model aided INS system in conjunction with a USBL and a DVL on a HUGIN 4500 AUV. Their results showed that the most accurate solution was developed using the fusion of all available data, but in the event the AUV was operating in the mid water column without DVL bottom lock or the USBL transmission rate was lowered, the more accurate hydrodynamic model significantly reduced the position error when compared to the INS only solution. Additionally, the algorithm developed also estimates the local current field which can be used to provide better DR solutions as well as provide data for physical oceanographic characteristics and mission path planning [5].

With electronic components such as micro-electromechanical system (MEMS) IMUs and AHRS decreasing in size and increasing in accuracy, small AUVs, on the order of two meters in length, are becoming common research tools due to their ease of portability and smaller cost. While the HUGIN 4500 AUV has the displacement and power capacity to support the use of a DVL and a USBL, a typical small AUV does not. Rypkema et al. designed and field tested a OWTT-iUSBL system for a Bluefin Sandshark AUV. Their results demonstrated the effectiveness of the system by reducing the error between GPS surfacing events by nearly a factor of two [11].

This thesis seeks to determine if a OWTT-iUSBL system coupled with a vehicle model and an AHRS can be used to determine the local current field as well as determine bias present in the vehicle speed measurement due to changes in hydrodynamic form. Implementing a software solution instead of the addition of an acoustic Doppler current profiler (ADCP) to measure the local current field conserves displacement and power capacity for additional payload, thus increasing mission effectiveness. Additionally, with the knowledge of local current field and bias parameters, the filter's model of vehicle motion matches

the true motion more closely and therefor the DR accuracy will be improved. This not only minimizes the effect on position accuracy if acoustic navigation information is unavailable, but also allows reducing the OWTT-iUSBL transmission rate while maintaining position accuracy, which reduces the computational load on the system thereby lowering power consumption and increasing endurance.

The remaining chapters of this paper are organized as follows. Chapter 2 discusses the construction of the converted measurements Kalman filter (CMKF) and simulation results using constant and variable current velocities. Chapter 3 tests the filter's sensitivity to measurement biases and discusses methods for calculating and correcting for the observed effects. Chapter 4 discusses the results of the field experiment, to include the conduct of data collection and processing and construction of multiple filters to handle a variety of measurement inputs. Chapter 5 outlines the experimental conclusions and recommendations for further research.

Chapter 2

Ideal Model and Simulation

2.1 General Kalman Filter discussion

The Kalman filter (KF) is a recursive least squares algorithm which uses a mathematical model of system dynamics along with knowledge of the previous state of the system to predict the current state. If measurements of system parameters are available, they are used to augment that prediction. The notation used follows that presented by Bar-Shalom et al[1].

The KF cycle of estimation, augmentation and prediction begins with calculating the estimate of the current state and the associated covariance given the previous state estimation and covariance:

$$\hat{\mathbf{x}}(\mathbf{k}+\mathbf{1}|\mathbf{k}) = \mathbf{F}(\mathbf{k})\hat{\mathbf{x}}(\mathbf{k}|\mathbf{k}) + \mathbf{G}(\mathbf{k})\mathbf{u}(\mathbf{k}) + \mathbf{v}(\mathbf{k}) \tag{2.1}$$

$$\mathbf{P}(\mathbf{k}+\mathbf{1}|\mathbf{k}) = \mathbf{F}(\mathbf{k})\mathbf{P}(\mathbf{k}|\mathbf{k})\mathbf{F}(\mathbf{k})' + \mathbf{Q}(\mathbf{k}) \tag{2.2}$$

where $\hat{\mathbf{x}}$ represents the state vector, $\mathbf{P}$ is the state covariance matrix, $\mathbf{F}$ is the state transition matrix, $\mathbf{u}$ is a control input vector, $\mathbf{G}$ is the associated gain matrix and $\mathbf{v}$ is the process noise vector assumed to be zero mean, white and Gaussian distributed with the following covariance:

$$E[\mathbf{v}(\mathbf{k})\mathbf{v}(\mathbf{k})'] = \mathbf{Q}(\mathbf{k}) \tag{2.3}$$

New measurements may not be available if the update rate of the filter is not matched to the update rate of the sensors, as might be the case with acoustic navigation. In that instance, the state estimate becomes the state prediction and the cycle repeats. If new measurements

are available, the predicted measurement vector is then calculated.

$$\hat{\mathbf{z}}(\mathbf{k+1}|\mathbf{k}) = \mathbf{H}(\mathbf{k+1})\hat{\mathbf{x}}(\mathbf{k+1}|\mathbf{k}) + \mathbf{w}(\mathbf{k}) \tag{2.4}$$

where $\hat{\mathbf{z}}$ represents the predicted measurement, $\mathbf{H}$ is the measurement mapping matrix and $\mathbf{w}$ is the measurement noise vector assumed to be zero mean, white and Gaussian distributed with the following covariance:

$$E[\mathbf{w}(\mathbf{k})\mathbf{w}(\mathbf{k})'] = \mathbf{R}(\mathbf{k}) \tag{2.5}$$

In order to obtain a metric which describes the degree of agreement between the measured value and the predicted measurement, the measurement prediction error or innovation and its associated covariance are calculated:

$$\boldsymbol{\nu}(\mathbf{k+1}) = \mathbf{z}(\mathbf{k+1}) - \hat{\mathbf{z}}(\mathbf{k+1}|\mathbf{k}) \tag{2.6}$$

$$\mathbf{S}(\mathbf{k+1}) = \mathbf{H}(\mathbf{k+1})\mathbf{P}(\mathbf{k+1})\mathbf{H}(\mathbf{k+1})' + \mathbf{R}(\mathbf{k+1}) \tag{2.7}$$

where $\boldsymbol{\nu}$ is the innovation, $\mathbf{z}$ is the measurement and $\mathbf{S}$ is the innovation covariance. In order to augment the predicted state with the information from the measurements, the state prediction covariance and the innovation covariance matrices are combined using the measurement mapping matrix to produce a gain or weighting matrix:

$$\mathbf{W}(\mathbf{k+1}) = \mathbf{P}(\mathbf{k+1}|\mathbf{k})\mathbf{H}(\mathbf{k+1})'\mathbf{S}(\mathbf{k+1})^{-\mathbf{1}} \tag{2.8}$$

where $\mathbf{W}$ is the filter gain. A study of the structure of the equation gives insight to the value of the gain because a covariance matrix reflects the filter's belief in the accuracy of the associated parameter. With the state estimate covariance in the numerator and the innovation covariance in the denominator, it can be seen that an inaccurate state prediction along with an accurate measurement will result in a large gain with the reverse true as well. Thus, if the filter gain is large, the state prediction will be influenced closer to the value of the more accurate measurements, while if the gain is small, the change in the predicted state vector will be small. Once the filter gain is calculated, the updated state prediction

and covariance matrix are calculated:

$$\hat{\mathbf{x}}(\mathbf{k+1}|\mathbf{k+1}) = \hat{\mathbf{x}}(\mathbf{k+1}|\mathbf{k}) + \mathbf{W}(\mathbf{k+1})\boldsymbol{\nu}(\mathbf{k+1}) \tag{2.9}$$

$$\begin{aligned}\mathbf{P}(\mathbf{k+1}|\mathbf{k+1}) &= [\mathbf{I} - \mathbf{W}(\mathbf{k+1})\mathbf{H}(\mathbf{k+1})]\mathbf{P}(\mathbf{k+1}|\mathbf{k}) \\ &[\mathbf{I} - \mathbf{W}(\mathbf{k+1})\mathbf{H}(\mathbf{k+1})]' + \mathbf{W}(\mathbf{k+1})\mathbf{R}(\mathbf{k+1})\mathbf{W}(\mathbf{k+1})'\end{aligned} \tag{2.10}$$

The state covariance matrix equation presented is known as the Joseph stabilized form. The mathematical construction of this form reduces rounding errors as compared to other methods and ensures that the state covariance matrix output will be positive definite as long as the input state covariance matrix is also positive definite although at higher computational cost. Crassidis and Junkins demonstrated that a positive definite state covariance matrix ensures filter stability[3].

The matrices $\mathbf{F}$, $\mathbf{G}$, $\mathbf{Q}$, $\mathbf{H}$ and $\mathbf{R}$ are assumed to be known and may vary with time. The initial state vector, $\hat{\mathbf{x}}(\mathbf{0})$ is assumed to be unknown and represented by a Gaussian distributed random variable with known mean and covariance. Additionally, the state vector, process noise and measurement noise are assumed to be independent. Under these assumptions, the KF is an optimal estimator in terms of the minimum mean squared error (MMSE). If the process and measurement noise are not Gaussian distributed, but the mean and covariance are known, as assumed above, then the KF is the best linear estimator in terms of MMSE[1]. These properties form the basis of the decision to use the KF as the estimator for this thesis.

2.1.1 Filter Consistency Testing

Testing filter consistency involves verifying the errors associated with the state and innovation vectors are zero mean and have covariance values matched to the error covariance matrix calculated by the filter. Because the error covariance matrix is used by the filter to determine the filter gain, validating consistency also validates that the filter is optimal as well[1].

First, the normalized estimation error squared (NEES) evaluates the assumptions for the state vector with an expected mean equal to the number of variables in the state vector. If the NEES indicates the filter is inconsistent as demonstrated by values outside of the acceptable confidence bounds, the normalized mean estimation error (NMEE) is used to

test the whiteness of each state variable individually. A persistent deviation from a mean of zero indicates the presence of a bias. Both of these tests require that the true values of the state variables at each step are known and therefore can only be used in simulation[1].

Similar to the NEES, the normalized innovation squared (NIS) verifies the consistency of the innovation vector with an expected mean equal to the number of variables in the measurement vector. As with the state vector, if the NIS indicates inconsistency, a sample auto-correlation test can be conducted to verify the statistics for each variable in the innovation vector. Unlike the state vector statistics, the innovation vector statistical tests only use filter calculated values and can be used to evaluate experimental data as well as in simulation.

2.2 Specific Filter Construction

As is common in navigation applications, the state vector contains Cartesian coordinates, such as the easting and northing components of position and velocity, while the measurements are reported in polar coordinates, in this case range and angle as well as speed and heading. Two options exist to handle the required conversion between coordinate systems to map the measurements to the state vector components. Either the state vector parameters are combined to convert to polar coordinates or the measurements are converted to Cartesian coordinates.

In the first case, a KF can not use the resulting non-linear equations and another method, such as the extended Kalman filter (EKF) must be used. The EKF uses a Taylor series expansion of up to second order of the non-linear state transition and/or measurement equations to produce a linearized approximation that is evaluated at the current predicted state. This process introduces bias from the linearization and error from evaluating at the current prediction instead of the actual state, which is not known. These biases and errors violate the assumptions of the KF and contribute to filter instability [1].

In the second case, converting the measurements to Cartesian coordinates allows the use of linear state transition and measurement equations, however, the covariance must be recalculated at each step using the current predicted state as it is now a non-linear function of the raw measurements and errors. Lerro and Bar-Shalom developed the CMKF to not only calculate the required covariance, but also to predict and correct for the bias introduced

by the linearization of the covariance calculations and error caused by the use of the current predicted state vice the actual state. Their results showed that the CMKF offered superior consistency and stability as compared to the EKF [8].

2.2.1 Plant Model

This thesis proposes an expansion of the CMKF that estimates the state and the unknown current vector parameters. To accomplish this, the state vector consisting of ground referenced position and water referenced velocity is augmented with the vector components of the local current field:

$$\hat{\mathbf{x}}(k) = \begin{bmatrix} e_g(k) \\ \dot{e}_w(k) \\ n_g(k) \\ \dot{n}_w(k) \\ \dot{e}_c(k) \\ \dot{n}_c(k) \end{bmatrix} \tag{2.11}$$

where e_g and n_g are the easting and northing components of geographic position, $\dot{e}_w$ and $\dot{n}_w$ are the easting and northing components of the water referenced velocity and $\dot{e}_c$ and $\dot{n}_c$ are the easting and northing components of the local current field.
The filter is based on the nearly constant velocity (NCV) model of linear motion that results in the following state transition equations:

$$e_g(k+1) = e_g(k) + \dot{e}_w(k)\Delta t + \dot{e}_c(k)\Delta t + v_1(k) \tag{2.12a}$$

$$\dot{e}_w(k+1) = \dot{e}_w(k) + v_2(k) \tag{2.12b}$$

$$n_g(k+1) = n_w(k) + \dot{n}_w(k)\Delta t + \dot{n}_c(k)\Delta t + v_3(k) \tag{2.12c}$$

$$\dot{n}_w(k+1) = \dot{n}_w(k) + v_4(k) \tag{2.12d}$$

$$\dot{e}_c(k+1) = \dot{e}_c(k) + v_5(k) \tag{2.12e}$$

$$\dot{n}_c(k+1) = \dot{n}_c(k) + v_6(k) \tag{2.12f}$$

Note that unlike a traditional KF used for navigation that only uses ground referenced position and velocity in the state vector, this filter combines the water referenced and current field velocities to determine the ground referenced velocity. Using Eqn 2.11 to define the

state transition matrix results in:

$$\mathbf{F} = \begin{bmatrix} 1 & \Delta t & 0 & 0 & \Delta t & 0 \\ 0 & 1 & 0 & 0 & 0 & 0 \\ 0 & 0 & 1 & \Delta t & 0 & \Delta t \\ 0 & 0 & 0 & 1 & 0 & 0 \\ 0 & 0 & 0 & 0 & 1 & 0 \\ 0 & 0 & 0 & 0 & 0 & 1 \end{bmatrix} \tag{2.13}$$

In a traditional NCV, the acceleration of the system is unknown and modelled as a zero mean, white, Gaussian distributed random variable with a specified standard deviation. This standard deviation is then mathematically combined with a gain matrix which describes the relationship between each state variable and the acceleration to determine the process noise covariance matrix, Q. This method does not allow for tuning the individual process noise standard deviation for each state variable, which is undesired. Instead, this model uses individual standard deviations for each term in the state vector and assumes the variables are uncorrelated resulting in a diagonal matrix Q:

$$\mathbf{Q} = \begin{bmatrix} \sigma^2_{position} & 0 & 0 & 0 & 0 & 0 \\ 0 & \sigma^2_{velocity} & 0 & 0 & 0 & 0 \\ 0 & 0 & \sigma^2_{position} & 0 & 0 & 0 \\ 0 & 0 & 0 & \sigma^2_{velocity} & 0 & 0 \\ 0 & 0 & 0 & 0 & \sigma^2_{current} & 0 \\ 0 & 0 & 0 & 0 & 0 & \sigma^2_{current} \end{bmatrix} \tag{2.14}$$

where σ_{xx} is the standard deviation of the process noise assumed for each state vector variable.

2.2.2 Measurement Model

In a CMKF, the measurements in polar coordinates are converted into Cartesian coordinates and then mapped to the appropriate variables in the estimated measurement vector. In this filter, the measurements include the range (r) and azimuth (ϕ) from the OWTT-iUSBL acoustic system, the water referenced speed (s^w) calculated by the main vehicle computer

as a function of propeller revolutions per minute (RPM) and the heading (ψ) from the AHRS.

The converted measurements are calculated as follows:

$$\mathbf{z^c}(\mathbf{k}) = \begin{bmatrix} r(k)cos(\phi(k)) \\ s^w(k)cos(\psi(k)) \\ r(k)sin(\phi(k)) \\ s^w(k)sin(\psi(k)) \end{bmatrix} \tag{2.15}$$

were z^c is the vector of measurements converted into Cartesian coordinates.

Converting from one coordinate system to another introduces a bias that must be accounted for to ensure the accuracy of the resulting measurements. In simulation, the true measurement values are known and the following equations are used to calculate the measurement bias:

$$\boldsymbol{\mu(k)} = \begin{bmatrix} r(k)cos(\phi(k))(e^{-\sigma_\phi^2/2} - 1) \\ s^w(k)cos(\psi(k))(e^{-\sigma_\psi^2/2} - 1) \\ r(k)sin(\phi(k))(e^{-\sigma_\phi^2/2} - 1) \\ s^w(k)sin(\psi(k))(e^{-\sigma_\psi^2/2} - 1) \end{bmatrix} \tag{2.16}$$

where r and s^w are the true measurement values.

The measurement noise is formed by first determining the eigenvalues and eigenvectors of $\mathbf{R}$, where the square root of the eigenvalue represents the variance for each measurement. The eigenvectors are then multiplied by the variance and a vector of random normal Gaussian distributed values.

Combining the converted measurements with the bias and the measurement noise results in the final measurement vector formulation:

$$\mathbf{z}(\mathbf{k}) = \mathbf{z^c}(\mathbf{k}) - \mu(\mathbf{k}) + \mathbf{w}(\mathbf{k}) \tag{2.17}$$

Because the measurement vector is now a non-linear combination of measurements, the covariance matrix of the vector is also a non-linear combination of the measurements and the associated errors. In simulation, the true measurement values are known and the following

equations are used to calculate the measurement covariances:

$$\begin{aligned} R_t^{11} =& r^2 e^{-\sigma_\phi^2}[cos^2(\phi)(cosh(\sigma_\phi^2) - 1) + sin^2(\phi)sinh(\sigma_\phi^2)] \\ &+ (\sigma_r^2 e^{-\sigma_r^2})[cos^2(\phi)cosh(\sigma_\phi^2) + sin^2(\phi) * sinh(\sigma_\phi^2)] \end{aligned} \tag{2.18a}$$

$$\begin{aligned} R_t^{22} =& s^{w^2} e^{-\sigma_\psi^2}[cos^2(\psi)(cosh(\sigma_\psi^2) - 1) + sin^2(\psi)sinh(\sigma_\psi^2)] \\ &+ (\sigma_{s^w}^2 e^{-\sigma_{s^w}^2})[cos^2(\psi)cosh(\sigma_\psi^2) + sin^2(\psi) * sinh(\sigma_\psi^2)] \end{aligned} \tag{2.18b}$$

$$\begin{aligned} R_t^{33} =& r^2 e^{-\sigma_\phi^2}[sin^2(\phi)(cosh(\sigma_\phi^2) - 1) + cos^2(\phi)sinh(\sigma_\phi^2)] \\ &+ (\sigma_r^2 e^{-\sigma_r^2})[sin^2(\phi)cosh(\sigma_\phi^2) + cos^2(\phi) * sinh(\sigma_\phi^2)] \end{aligned} \tag{2.18c}$$

$$\begin{aligned} R_t^{44} =& s^{w^2} e^{-\sigma_\psi^2}[sin^2(\psi)(cosh(\sigma_\psi^2) - 1) + cos^2(\psi)sinh(\sigma_\psi^2)] \\ &+ (\sigma_{s^w}^2 e^{-\sigma_{s^w}^2})[sin^2(\psi)cosh(\sigma_\psi^2) + cos^2(\psi) * sinh(\sigma_\psi^2)] \end{aligned} \tag{2.18d}$$

$$R_t^{13} = R_t^{31} = sin(\phi)cos(\phi)e^{-2\sigma_r^2}[\sigma_r^2 + r^2(1 - e^{\sigma_\phi^2})] \tag{2.18e}$$

$$R_t^{24} = R_t^{42} = sin(\psi)cos(\psi)e^{-2\sigma_{s^w}^2}[\sigma_{s^w}^2 + s^{w^2}(1 - e^{\sigma_\psi^2})] \tag{2.18f}$$

where R_t^{xx} is the covariance parameter evaluated using true measurement values and σ_{xx} represents the standard deviation of the specified parameter.

With the polar measurements and covariances converted to Cartesian coordinates, a linear measurement mapping matrix is used to calculate the innovation covariance and filter gain:

$$\mathbf{H} = \begin{bmatrix} 1 & 0 & 0 & 0 & 0 & 0 \\ 0 & 1 & 0 & 0 & 0 & 0 \\ 0 & 0 & 1 & 0 & 0 & 0 \\ 0 & 0 & 0 & 1 & 0 & 0 \end{bmatrix} \tag{2.19}$$

Using separate variables for the water referenced velocity and current velocity to represent the ground referenced velocity coupled with a ground referenced position source and water referenced velocity measurements allows the filter to calculate the values of the components of current velocity that correspond to the changes in range based on the acoustic position measurement.

2.3 Current Estimation Simulations

To verify filter function, accuracy and consistency, a series of Monte Carlo simulations was performed. Each simulation consisted of 10 runs of two steady course legs with a 180 degree turn in the middle of the mission. The 180 degree turn tests whether or not the filter is calculating current correctly by demonstrating that the steady course values do not significantly change. The track represents a one hour mission to allow the simulated vehicle to open range from the source to observe the range dependent error characteristics inherent to the conversion from polar coordinate measurements to Cartesian coordinate state vector values. An update rate of one Hz was chosen as a realistic value of OWTT-iUSBL update rate in the field.

For each set of conditions, the filter position output and calculated current are evaluated against the input values to determine accuracy. Additionally, the filter must also be consistent as demonstrated by showing that the state vector and the innovation are both unbiased and that error statistics match those assumed in the filter construction. For the state vector, the NEES and the NMEE test the assumption of consistency and for the innovation, the NIS is used [1]. The standard deviations for the various stochastic parameters are summarized in Table 2.1.

Table 2.1: Standard Deviations of Various Variables

Parameter	Value
$\sigma_{position}$	0.6 m
$\sigma_{velocity}$	0.4 m/s
$\sigma_{current}$	0.1 m/s
σ_r	1 m
σ_ϕ	0.6 deg
σ_{s^w}	.5 m/s
σ_ψ	.6 deg

Two sections are presented: constant current and diurnal varying current.

2.3.1 Constant

A constant current with magnitude 0.25 m/s and direction of 60 degrees affects the vehicle throughout the simulation. Figure 2-2a shows the filter geographic position output compared to the ground truth of the simulation. The filter output accurately represents the position

of the vehicle while displaying noisy characteristics but no bias. This response is expected based on the construction of the filter measurements consisting of the ground truth values combined with additive zero mean Gaussian distributed white noise.

Figure 2-3a shows the difference between the actual range and the range calculated using the easting and northing position components of the state vector. The filter output error remains less than 10 meters in range for the duration of the simulation. After the filter converges on a reasonable value for the current, the error in azimuth remains less than 2 degrees for the remainder of the simulation. Additionally, the magnitude of the range error increases as range increases and decreases as range is reduced which is expected based on the range dependent nature of the error in the converted measurements.

With an initialized current value of zero, the filter determines the correct magnitude and direction of current approximately five minutes into the simulation. The current value is initialized to zero to demonstrate that if the filter requires re-initializing during the mission when the actual current will not be available, the filter will be able to function properly. Figure 2-2b shows that the characteristics of the calculations do not appreciably change after the turn at 1800 seconds. Although the instantaneous value of the magnitude and direction are noisy, the mean values over the course of the mission of 0.26 m/s and 59.3 degrees agree closely with the simulation parameters.

The state covariance matrix contains the information that represents the filter's belief in the quality of the estimation. One way to visualize this information is to calculate the L2 norm of the matrix. A small norm represents that the filter believes the estimate is good with the opposite being true as well. Figure 2-3b shows the error covariance matrix norm exhibiting range dependent characteristics, which is expected.

Figure 2-4a shows that the filter is initially optimistic (less accurate than it thinks it is) as demonstrated by the plotted values above the upper 99% line. This is due to the current velocity being initialized at zero when the actual value was non-zero. As the current value is reasonably determined, the filter becomes pessimistic before the turn is made when the filter becomes consistent. The mean of this value should be equal to the number of state variables, and at 5.9043, this agrees closely.

Figure 2-1 shows that the error statistics of the innovation are consistent and steady throughout the run. The mean of the NIS should be equal to the number of variables in the measurement vector, and at 3.5317, this agrees well.

As a test of the whiteness of the estimation of the state, the normalized mean estimation error should stay within the displayed 95% confidence bounds. As shown in Figure 2-4b, each of the state variables displays appropriate characteristics throughout the run.

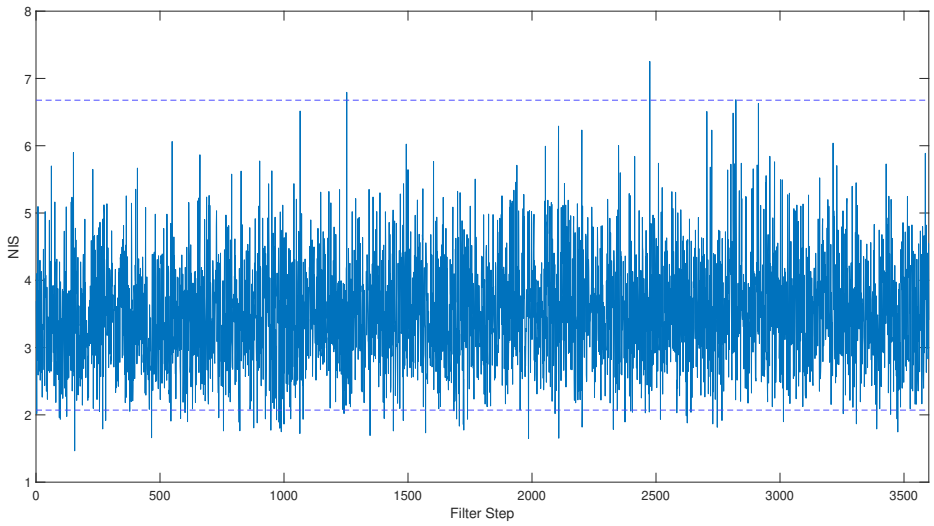

Figure 2-1: Innovation vector statistic with constant current and unbiased inputs. The NIS demonstrates the innovation vector is consistent throughout the simulation.

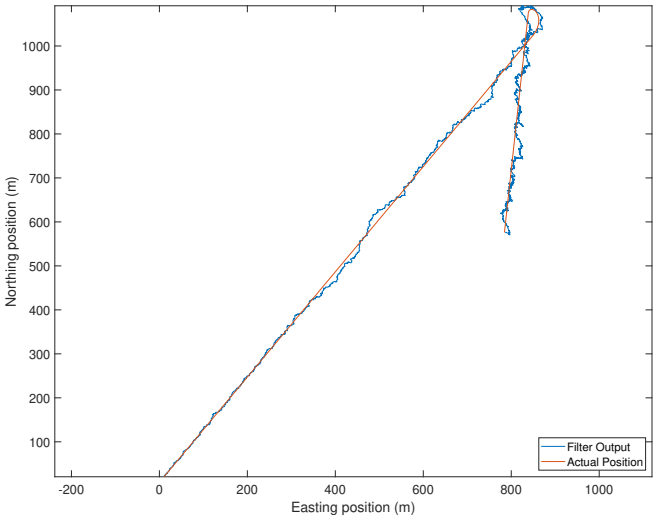

(a) Actual vs Filter Output Position

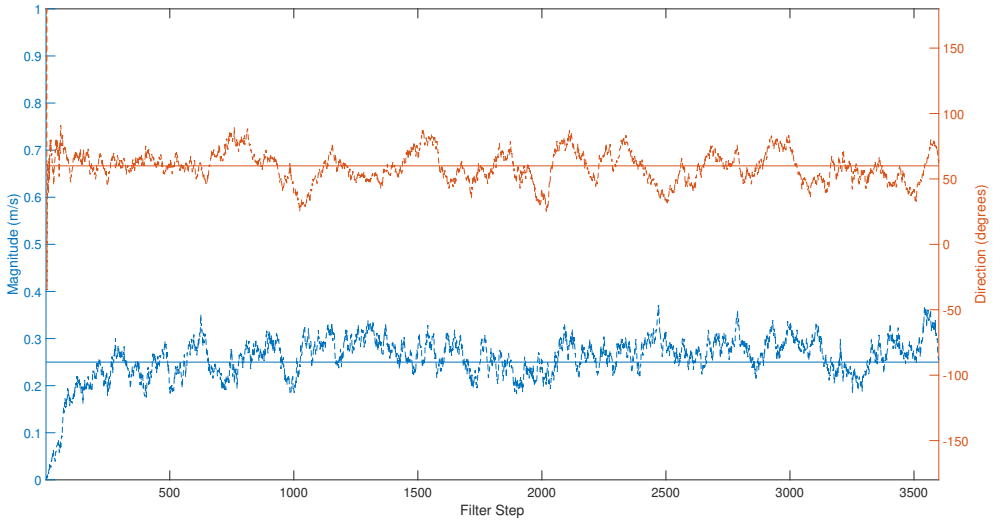

(b) Calculated Current Magnitude and Direction vs Filter Step

Figure 2-2: Filter outputs of position and current magnitude and direction with constant current and unbiased inputs. With the current velocity initialized at zero, the filter requires less than 500 steps to achieve a reasonable estimation of the actual current velocity.

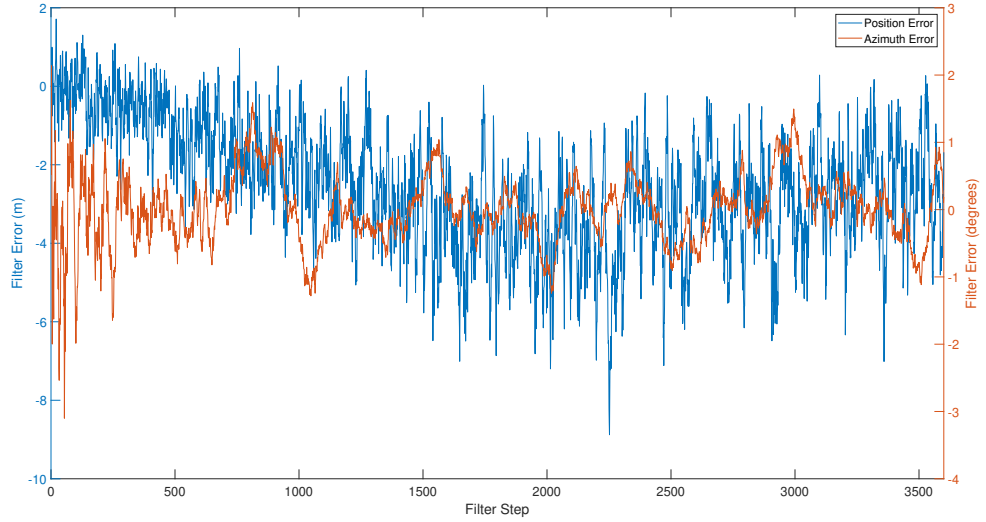

(a) Filter Error vs Filter Step

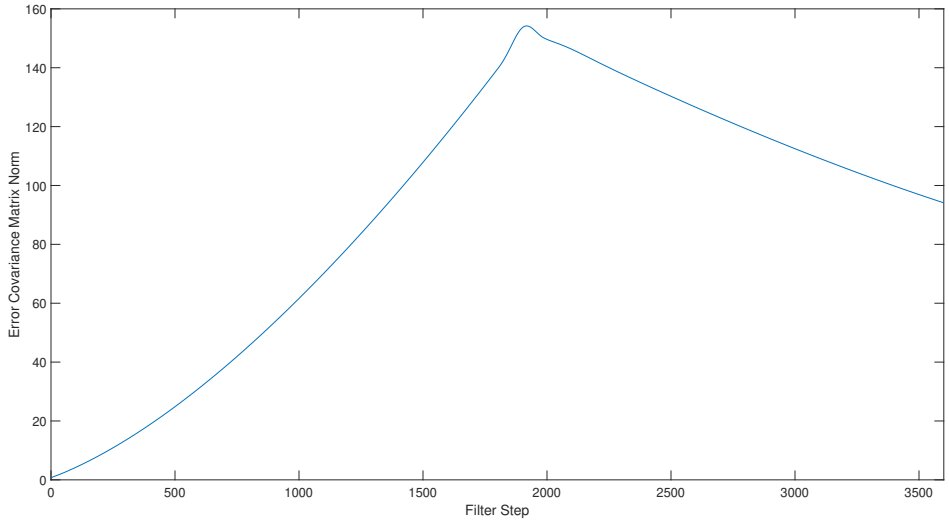

(b) Process Error Covariance Norm vs Filter Step

Figure 2-3: Filter error versus filter step and process noise covariance matrix norm with constant current and unbiased inputs. Note the range dependent characteristics of the range error and the value of the norm.

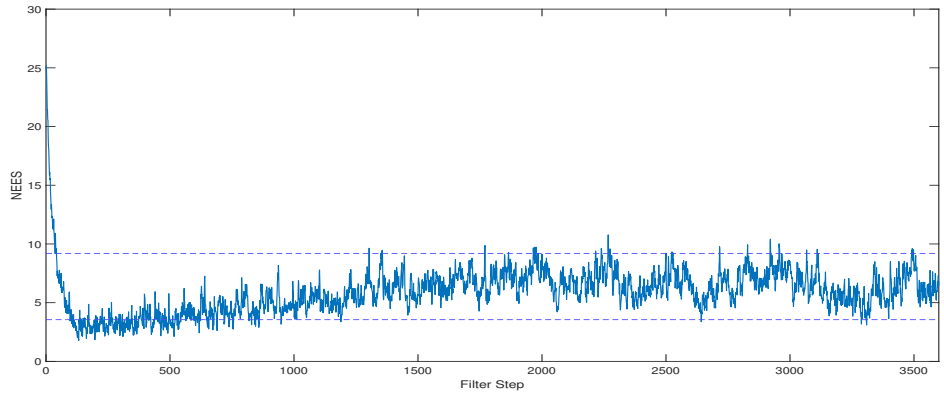

(a) 10 Run Normalized Estimation Error Squared (NEES)

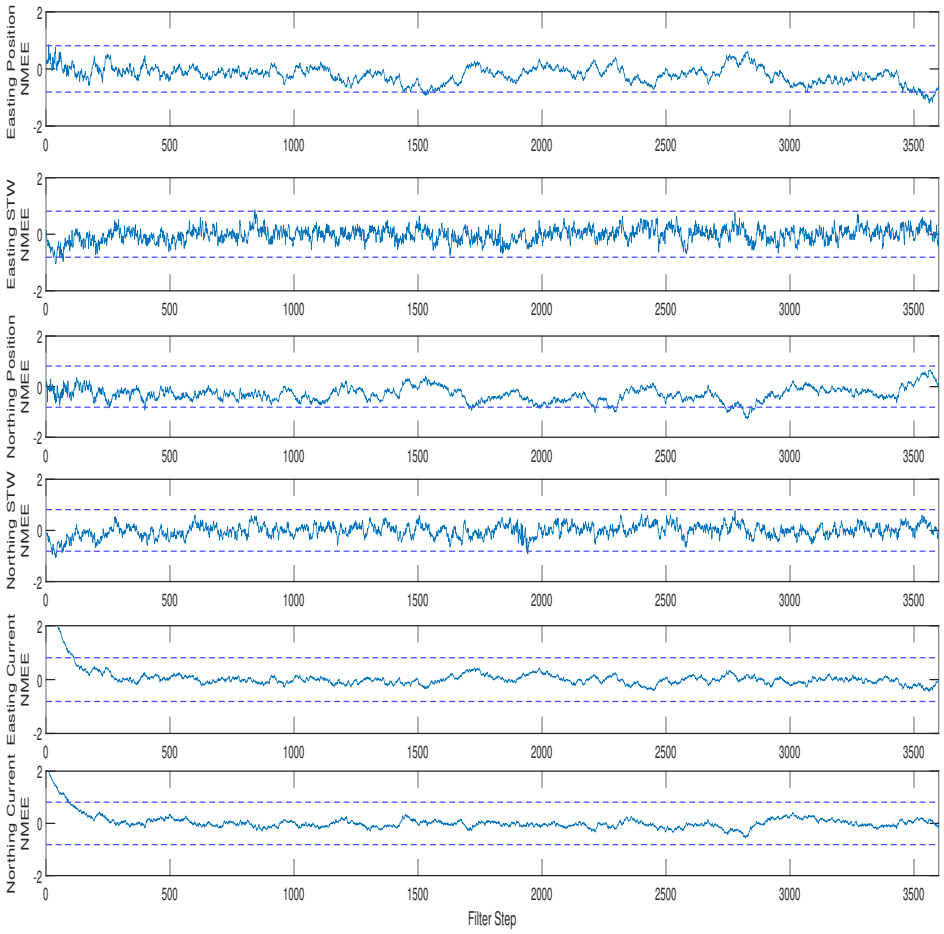

(b) Normalized Mean Estimation Error (NMEE)

Figure 2-4: State vector statistics with constant current and unbiased inputs. The values of both the NEES and the NMEE show that once a reasonable estimate of current velocity is determined, the filter achieves consistency across all state vector variables.

2.3.2 Slowly changing, periodic

In this simulation, the current is no longer held constant in magnitude, but varies slowly to test the filter's ability to react to changing conditions. The applied current has a constant direction, but the magnitude follows a sine function with 12 hour period and a 0.5 m/s amplitude. Although the state transition matrix assumes the current velocity is constant, the non-zero covariance value allows the filter to estimate the parameter if the change is slow[1].

As with the constant current case, Figures 2-6a and 2-7a demonstrate that the filter maintains an accurate estimation of position with a maximum range error of eight meters and an angle error of less than two degrees once the filter has stabilized. Also, the expected range dependent nature of the range error can again be observed similar to the previous simulation.

As shown in Figure 2-6b, the filter resolves the correct direction with the correct magnitude following after approximately 300 filter steps or 5 minutes at the simulated transmission rate of 1 Hz. The calculated magnitude then continues to track with the value of the simulated current field.

The remaining figures demonstrated characteristics similar to the previously presented case but are included for completeness.

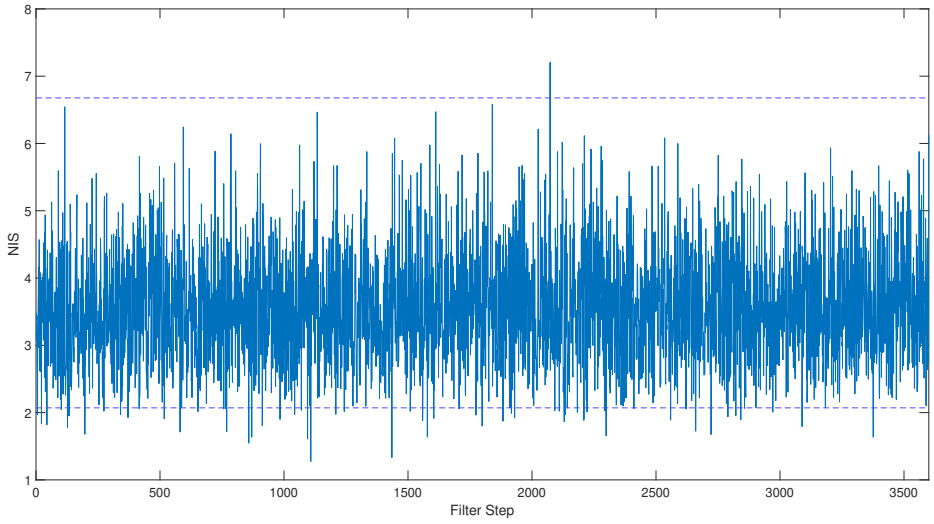

Figure 2-5: Innovation vector statistic with variable current and unbiased inputs. The NIS demonstrates the innovation vector is consistent throughout the simulation.

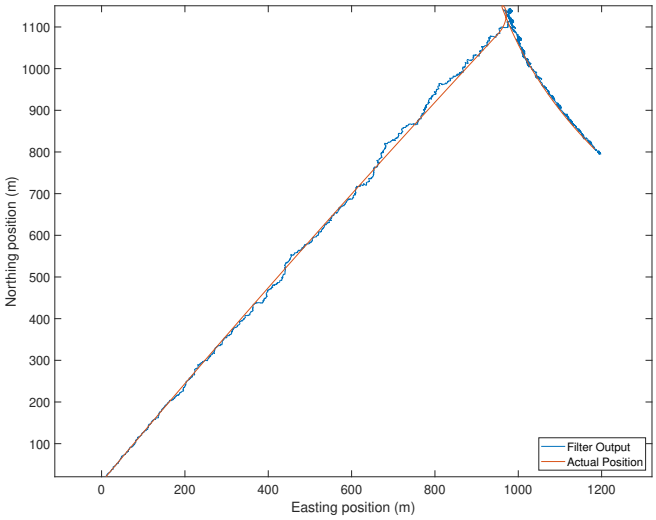

(a) Actual vs Filter Output Position

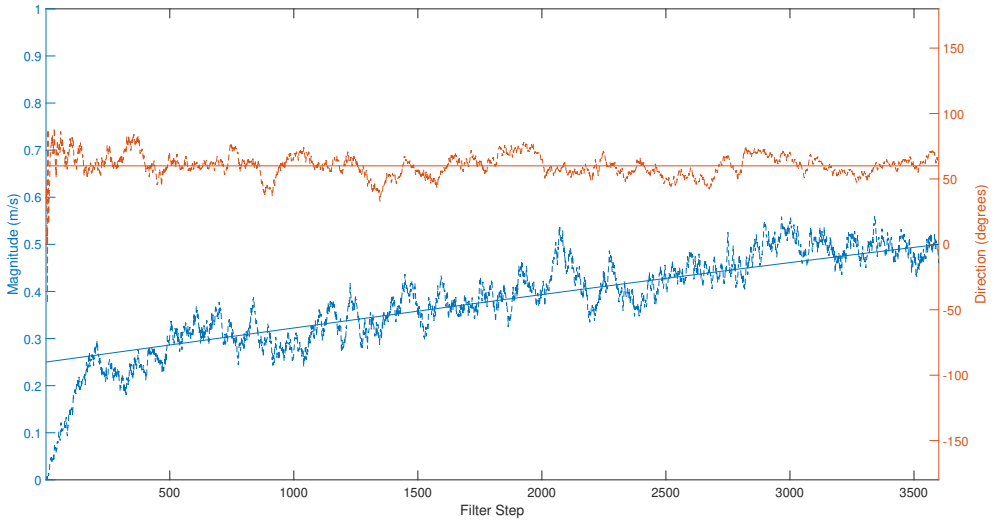

(b) Calculated Current Magnitude and Direction vs Filter Step

Figure 2-6: Filter outputs of position and current magnitude and direction with variable current and unbiased inputs. As with the constant current case, the filter requires less than 500 steps to achieve a reasonable estimation of the actual current velocity.

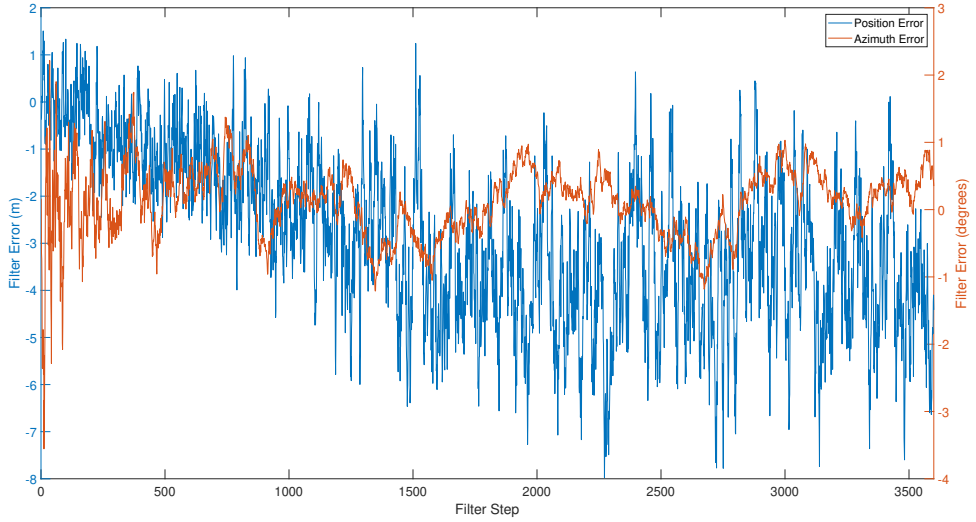

(a) Filter Error vs Filter Step

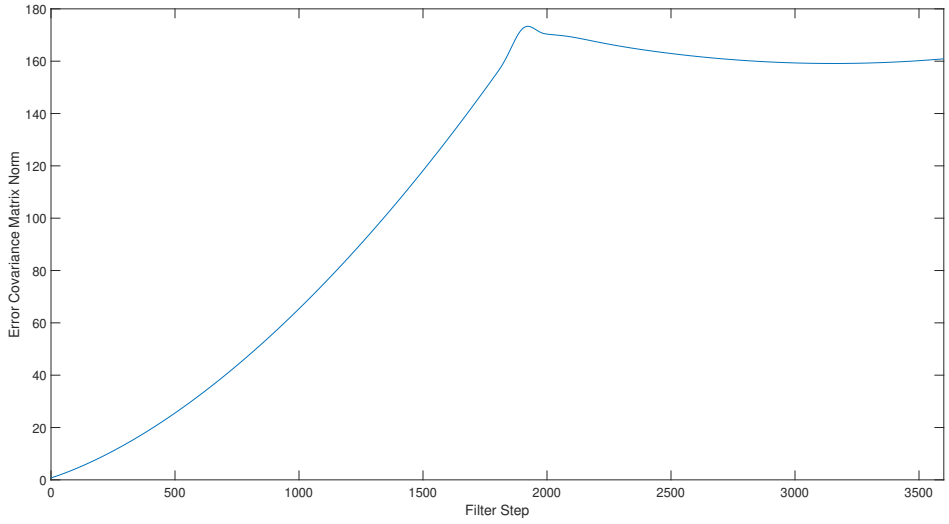

(b) Process Error Covariance Norm vs Filter Step

Figure 2-7: Filter error versus filter step and process noise covariance matrix norm with variable current and unbiased inputs. Again, the simulation shows the range dependent characteristics of the range error and the value of the norm.

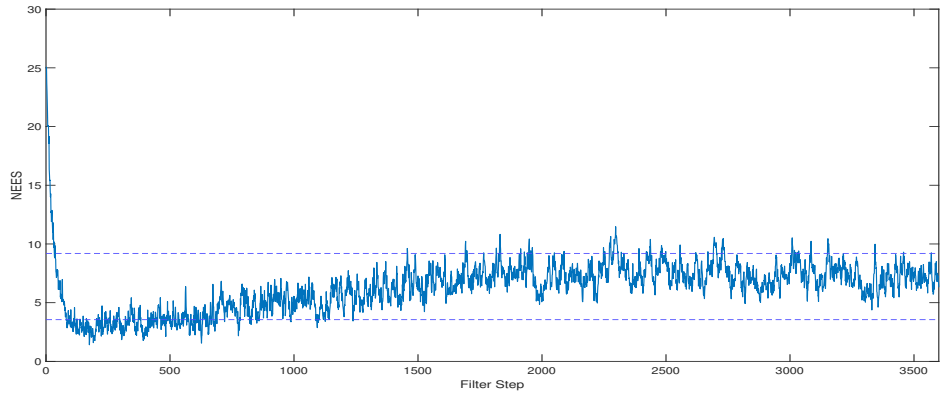

(a) 10 Run Normalized Estimation Error Squared (NEES)

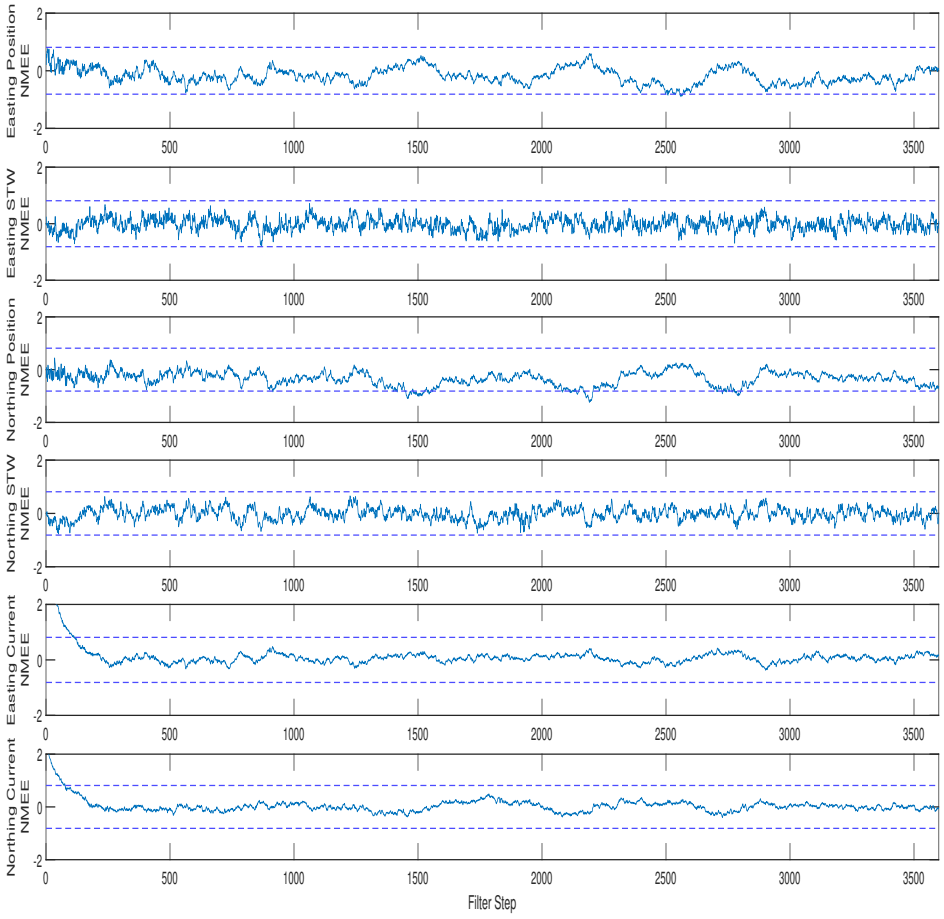

(b) Normalized Mean Estimation Error (NMEE)

Figure 2-8: State vector statistics with variable current and unbiased inputs. The values of both the NEES and the NMEE show that once a reasonable estimate of current velocity is determined, the filter achieves consistency across all state vector variables.

Chapter 3

Filter Performance with Non-Ideal Inputs

3.1 Sensitivity to Measurement Biases

The previous chapter demonstrated that with measurements which are unbiased and conform to a normal distribution, the filter output is also unbiased and the stochastic characteristics are consistent with the values used to generate the white noise. In practice, error will be introduced into the filter output due to real signals being neither unbiased nor normally distributed. In this chapter, sources of noise and bias will be considered and, for those that cannot be neglected, compensation methods will be explored.

Measurement noise which is not actually white can be accounted for by using larger values for the covariances of the various measurement vector components. Increasing the measurement covariance lowers the filter gain to reduce the weighing of the present measurement and increase the weighting of the present state estimate, which minimizes the effect of data with noise that does not conform to the assumptions of the KF on state estimation, but, if the present state estimate does not include reasonable values of the current velocity, the accuracy of the filter output will be detrimentally affected[1].

Bias, as indicated by a consistent offset of a measurement from the actual value, cannot be compensated for by changing covariances and may be accounted for by adding an element to the state vector to track and predict the bias from step to step [1]. Additionally, because of the conversion from polar to Cartesian coordinates, a bias in one measurement will affect

more than one state variable.

In acoustic positioning measurements, the main sources of bias are errors in the measurements of element locations and the actual sound speed profile diverging from the assumptions used in the processing algorithm. In the field tests presented in Chapter 4, the AUV operated at a depth of approximately three meters and, assuming the water column was well mixed to that depth, the sound speed variability as a function of depth will be neglected. The locations of the array elements were measured with millimeter accuracy which minimizes the effects of any bias generated by differences between modeled and actual hydrophone locations.

The water-referenced speed measurement from the main vehicle navigation system is calculated using a function of the propeller RPM determined by the manufacturer prior to delivery. While this method works well for an unmodified body, research teams typically attach various instruments and sensors to the AUV, thus changing the hydrodynamic drag. At this point, a given propeller RPM no longer results in the same actual speed which results in a biased calculation.

In the heading measurement from the AHRS, the major sources of error are magnetic distortion caused by hard and soft iron effects and gyro drift over time. Hard and soft iron calibration procedures can be carried out prior to deployment to minimize the impact of magnetic effects. Gyro drift is compensated for in the software package for the AHRS. These calibrations and corrections reduce the cumulative effect of the potential biases, resulting in a heading output error on the order of 1 to 2 degrees [9].

Based on the above discussion, the acoustic navigation system will be considered noisy, but unbiased and the errors associated with any actual bias will be neglected. The speed and heading measurements have the potential to introduce computationally significant errors into the filter output and the effects of these errors will be investigated in the following sections. Bias values for testing of 0.1 m/s and 2 degrees were chosen as realistic estimates based on evaluation of historical data.

3.1.1 0.1 m/s Speed Bias

In the following section, 0.1 m/s is added to the water referenced speed measurement to produce a 20% speed bias which simulates a difference in hydrodynamic drag between the factory calibrated vehicle state and actual deployment configuration. Over the short term, the expected value of the speed bias is assumed to be relatively constant as the physical construction of the vehicle will not change during the duration of the simulation.

As shown in Figures 3-2a and 3-3a, despite the bias introduced into the heading measurement, the position output remains accurate with respect to ground truth. This behavior is expected as the major driver of position calculation is the range and angle measurements from the acoustic navigation system.

In Figure 3-2b, the effect of the bias can clearly be seen. Prior to the turn, the filter underestimates the magnitude of the current because of the erroneously high water referenced speed. After the turn, the filter overestimates the magnitude of the current by roughly the same amount due to the fact that while the magnitude of the error remains unchanged, the direction is reversed and has the opposite effect on the calculations. After the turn, the calculated direction of the current stabilizes at a value somewhat different than the correct value because with the incorrect magnitude of the water referenced velocity vector, the current vector required to match the change in distance over time from the range and angle measurements will have a different direction as well as magnitude from the true vector.

The magnitude of the error covariance matrix in Figure 3-3b appears similar to the unbiased case, which is expected as the statistics of the process noise are unchanged by the bias. In contrast, the plot of the NEES in Figure 3-4a shows a larger mean and increased number of data points outside the 99% confidence bounds indicating that the biased filter is optimistic and less consistent than the unbiased filter. The higher mean value of the NEES could be caused by either a statistical mismatch between the filter and the data or the presence of a bias. A review of Figure 3-4b shows the normalized error for the velocity components of the state vector varies from one side of the 95% confidence band to the other, indicating that the filter output is biased.

As opposed to the NEES, the NIS in Figure 3-1 does not appear to be affected by the bias. The position state vector components are compared to the range and angle measurements, which are unbiased, and therefore the range and angle components of the NIS should

be unaffected. The filter believes the measured speed is accurate and drives the filter output to values that are actually incorrect, but consistent with the measurement and therefore, the speed component of the NIS is not affected. With erroneous velocity components, the calculated heading should fail to adequately compare with the measured value, however, the statistics appear to remain consistent. This warrants further testing.

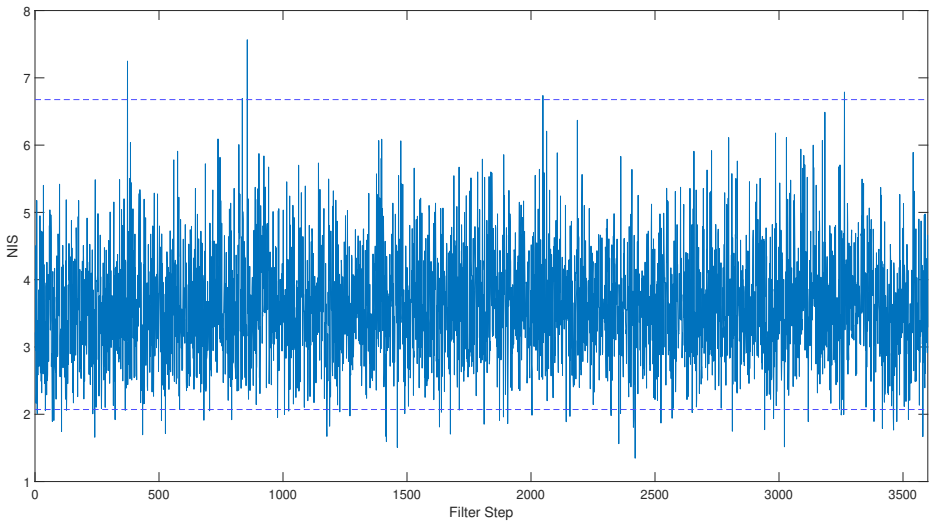

Figure 3-1: Innovation vector statistic with constant current and a speed bias of 0.1 m/s. The NIS demonstrates the innovation vector is consistent throughout the simulation, which was unexpected due to the intentionally incorrect speed measurement.

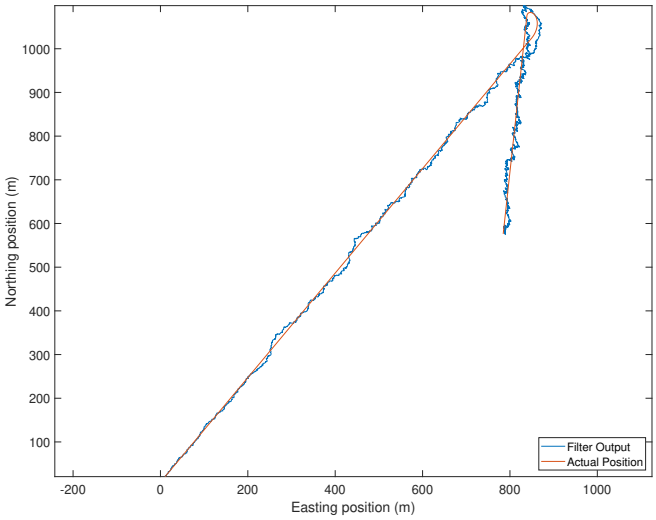

(a) Actual vs Filter Output Position

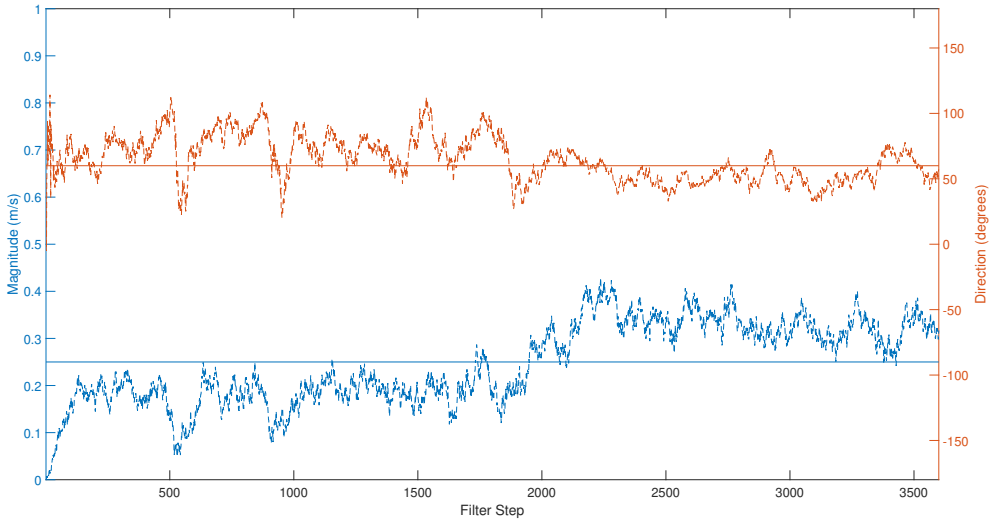

(b) Calculated Current Magnitude and Direction vs Filter Step

Figure 3-2: Filter outputs of position and current magnitude and direction with constant current and a speed bias of 0.1 m/s. Although the position output is unaffected due to the range and angle being unbiased, without knowledge of the bias, the filter calculated magnitude and direction of the current are offset from the true values both before and after the turn.

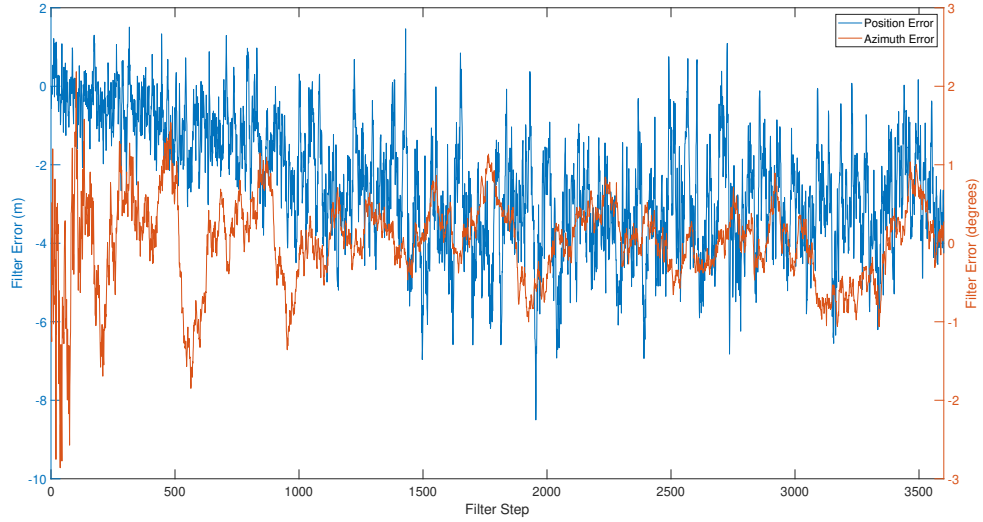

(a) Filter Error vs Filter Step

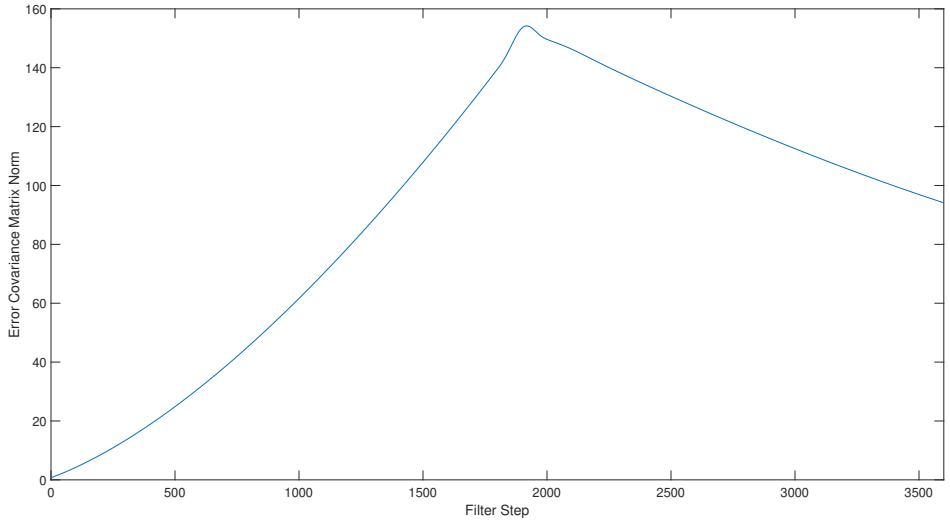

(b) Process Error Covariance Norm vs Filter Step

Figure 3-3: Filter error versus filter step and process noise covariance matrix norm with constant current and a speed bias of 0.1 m/s. As in the unbiased case, the simulation shows the range dependent characteristics of the range error and the value of the norm.

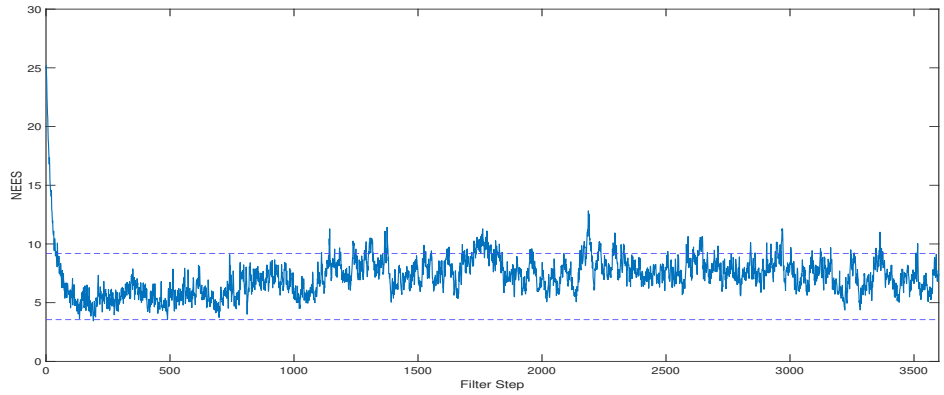

(a) 10 Run Normalized Estimation Error Squared (NEES)

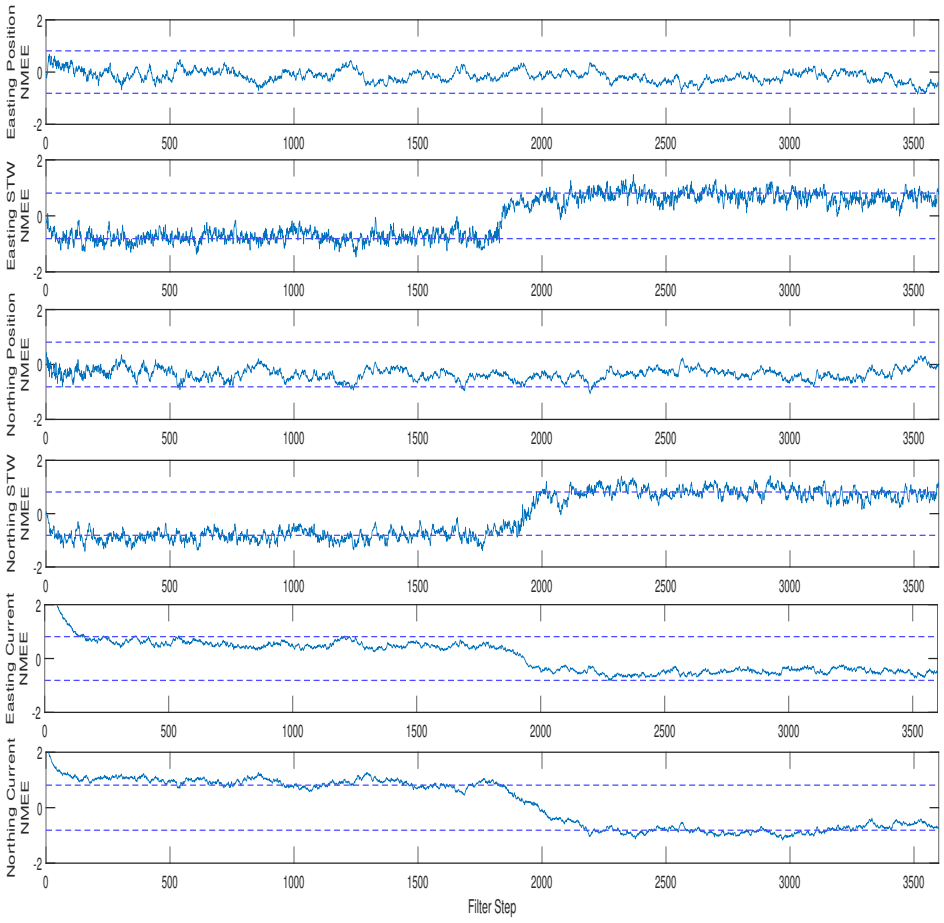

(b) Normalized Mean Estimation Error (NMEE)

Figure 3-4: State vector statistics with constant current and a speed bias of 0.1 m/s. The NEES shows the filter to be slightly optimistic, while the bias is clearly present in the plots of NMEE as shown by the significant deviation from zero in all state variables.

3.1.2 2 Degree Heading Bias

In the figures below, a 2 degree bias was introduced into the heading angle to evaluate the magnitude of error generated.

As in the previous bias example, the filter position output remains consistent with the actual track and does not does not demonstrate significant effects from the bias. Additionally, the filter error as a function of filter step shows similar characteristics to the unbiased case.

In Figure 3-6b, the bias in the angle causes the filter to slightly underestimate the magnitude of the current prior to the turn and overestimate after the turn. While the effect is noticeable, the magnitude of the error is smaller than that produced by the 0.1 m/s speed error.

Figure 3-8a shows that the bias has a minor effect on the NEES and the filter remains consistent. Figure 3-8b illustrates the bias effect on the velocity components of the state vector, although the statistics remain inside the 95% confidence bounds.

The remaining figures demonstrated similar behavior to the previously presented case but are included for completeness.

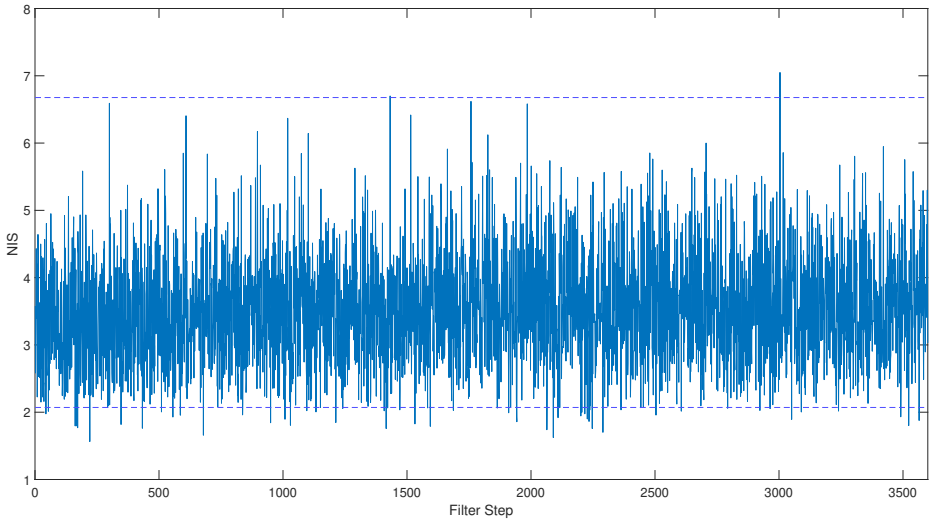

Figure 3-5: Innovation vector statistic with constant current and an angle bias of 2 degrees. The NIS demonstrates the innovation vector is consistent throughout the simulation, which was unexpected due to the intentionally incorrect angle measurement.

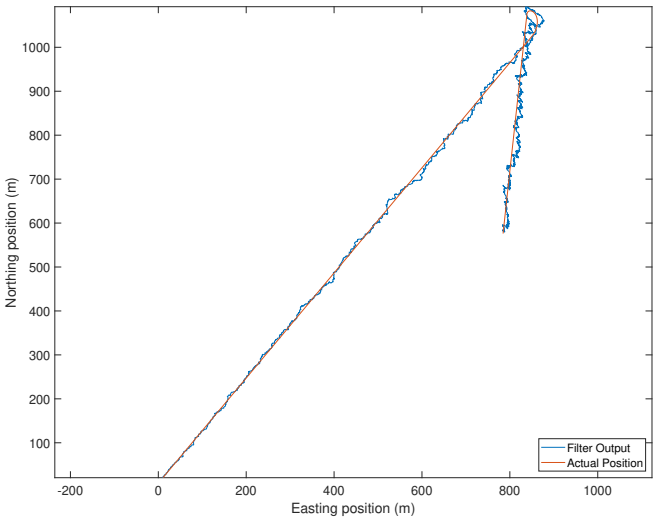

(a) Actual vs Filter Output Position

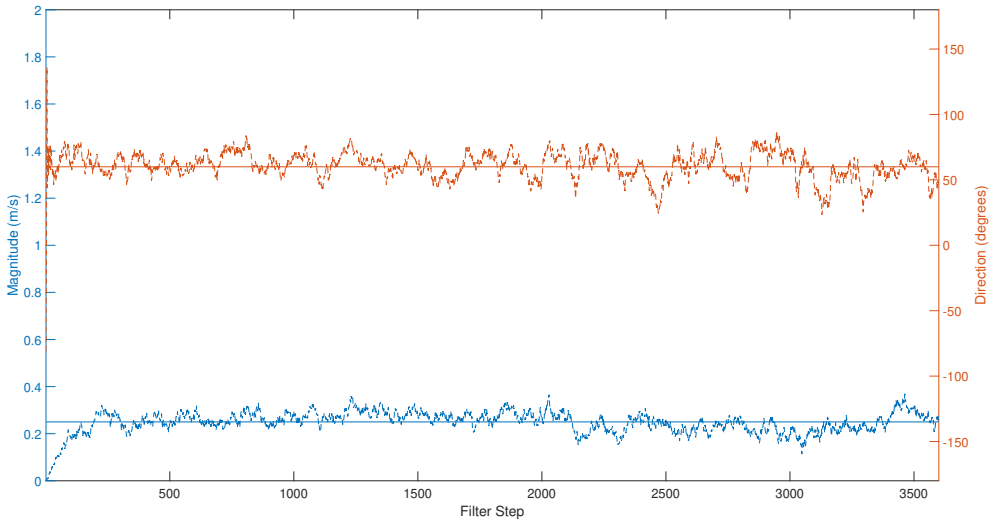

(b) Calculated Current Magnitude and Direction vs Filter Step

Figure 3-6: Filter outputs of position and current magnitude and direction with constant current and an angle bias of 2 degrees. The position output remains accurate despite the angle bias and the filter calculated magnitude and direction of the current demonstrate a small offset from the true values both before and after the turn.

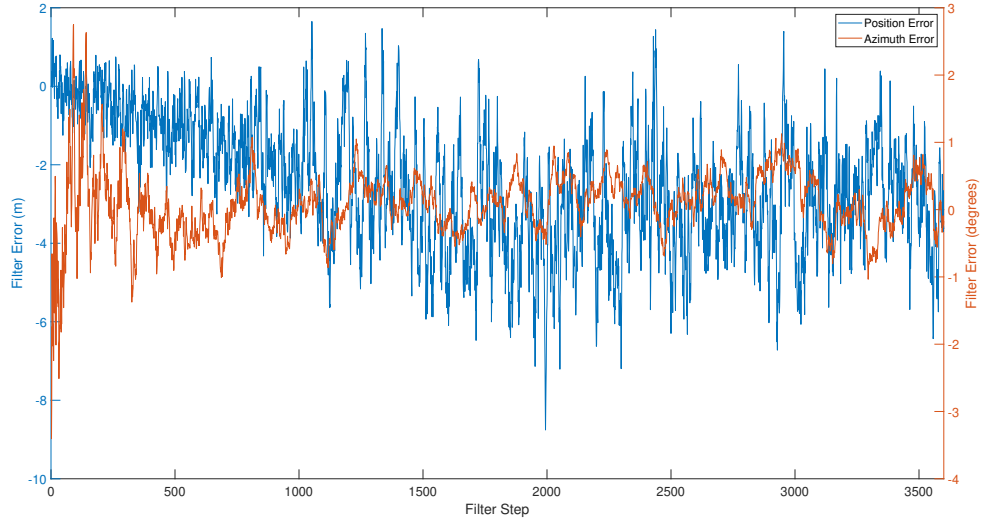

(a) Filter Error vs Filter Step

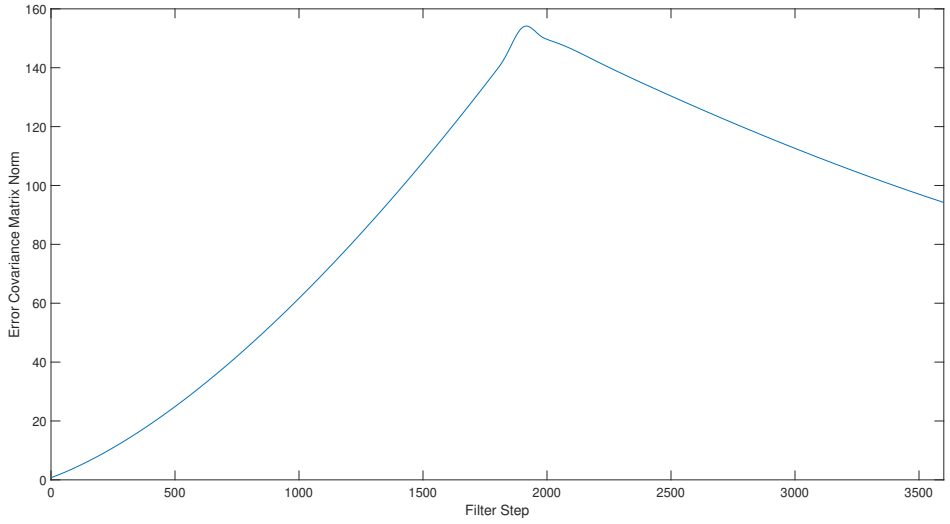

(b) Process Error Covariance Norm vs Filter Step

Figure 3-7: Filter error versus filter step and process noise covariance matrix norm with constant current and an angle bias of 2 degrees. As in the unbiased case, the simulation shows the range dependent characteristics of the range error and the value of the norm.

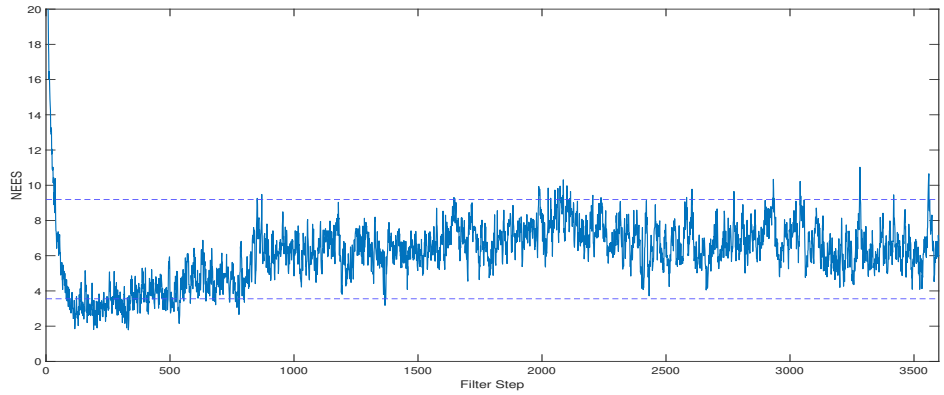

(a) 10 Run Normalized Estimation Error Squared (NEES)

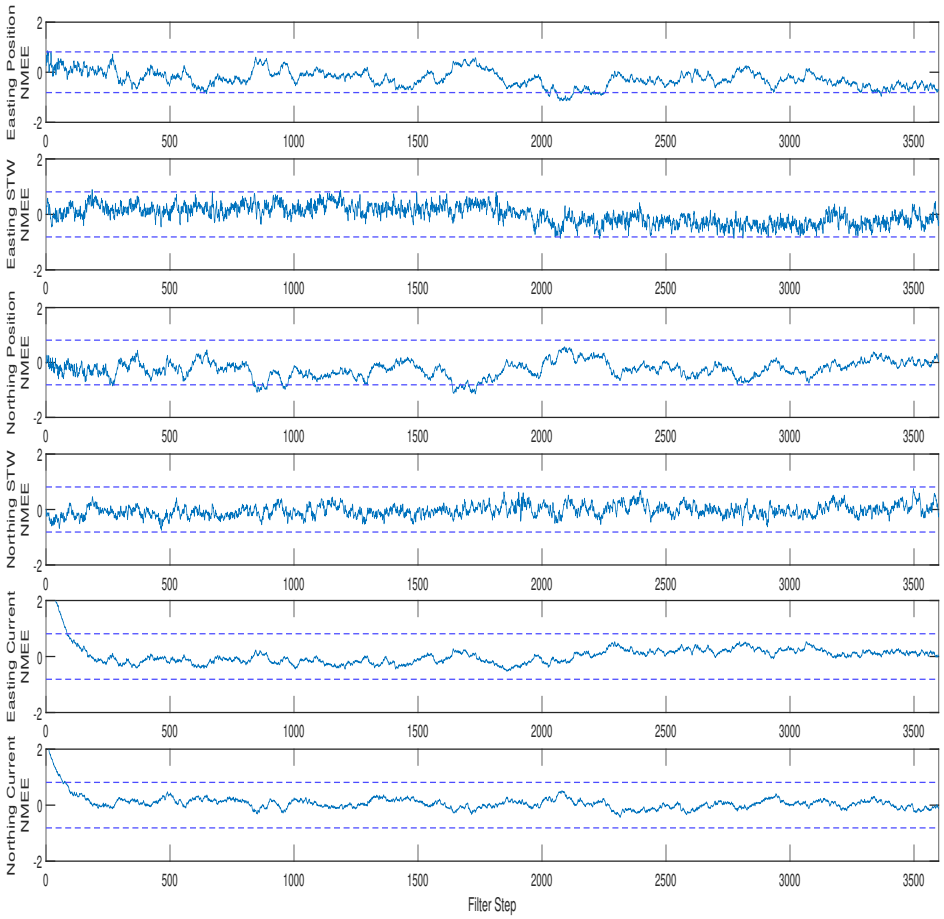

(b) Normalized Mean Estimation Error (NMEE)

Figure 3-8: State vector statistics with constant current and an angle bias of 2 degrees. Despite the angle bias, the NEES indicates the filter is consistent and while the values in the plots of the NMEE deviate from zero, they remain inside the 95% confidence bounds.

3.2 Bias Correction

Evaluation of the testing in the previous section indicates that the speed bias demonstrates a more prominent effect than the angle bias. This behavior is expected due to the current velocity calculations being more sensitive to small errors in speed than in heading. For example, if the reported speed contains a 0.1 m/s bias, the calculated current velocity will also be biased by the same amount. With the heading angle however, a 2 degree error in heading does not translate directly to a 2 degree error in the current direction due to the trigonometric nature of the calculations. Because of this, this thesis will consider the angle bias negligible and focus on a method to compensate for the speed.

In order to calculate and correct for the bias introduced to the speed measurement, several changes to the filter construction were required. First, a bias term was added to the state vector and defined as the ratio of the measured speed reported by the front seat navigation system and the actual speed.

$$b = \frac{s^w_{measured}}{s^w_{actual}} \tag{3.1}$$

Secondly, the converted measurements approach no longer works for the water referenced speed and heading measurements as the measured speed must be combined with the bias. To solve this issue, the state variables for easting and northing water referenced velocity and the bias term are combined in a non-linear measurement equation to create a filter which is a hybrid of converted measurements and EKF. As a result, the standard deviations, state vector, state transition matrix and process noise covariance matrix are as follows:

Table 3.1: Standard Deviations of Various Variables with Simulated Bias

Parameter	Value
$\sigma_{position}$	0.6 m
$\sigma_{velocity}$	0.3 m/s
$\sigma_{current}$	0.01 m/s
σ_{bias}	0.001 m/s
σ_r	1 m
σ_ϕ	0.6 deg
σ_{s^w}	1.5 m/s
σ_ψ	.6 deg

$$\hat{\mathbf{x}}(k) = \begin{bmatrix} e_g(k) \\ \dot{e}_w(k) \\ n_g(k) \\ \dot{n}_w(k) \\ \dot{e}_c(k) \\ \dot{n}_c(k) \\ b(k) \end{bmatrix} \tag{3.2}$$

$$\mathbf{F} = \begin{bmatrix} 1 & \Delta t & 0 & 0 & \Delta t & 0 & 0 \\ 0 & 1 & 0 & 0 & 0 & 0 & 0 \\ 0 & 0 & 1 & \Delta t & 0 & \Delta t & 0 \\ 0 & 0 & 0 & 1 & 0 & 0 & 0 \\ 0 & 0 & 0 & 0 & 1 & 0 & 0 \\ 0 & 0 & 0 & 0 & 0 & 1 & 0 \\ 0 & 0 & 0 & 0 & 0 & 0 & 1 \end{bmatrix} \tag{3.3}$$

$$\mathbf{Q} = \begin{bmatrix} \sigma^2_{position} & 0 & 0 & 0 & 0 & 0 & 0 \\ 0 & \sigma^2_{velocity} & 0 & 0 & 0 & 0 & 0 \\ 0 & 0 & \sigma^2_{position} & 0 & 0 & 0 & 0 \\ 0 & 0 & 0 & \sigma^2_{velocity} & 0 & 0 & 0 \\ 0 & 0 & 0 & 0 & \sigma^2_{current} & 0 & 0 \\ 0 & 0 & 0 & 0 & 0 & \sigma^2_{current} & 0 \\ 0 & 0 & 0 & 0 & 0 & 0 & \sigma^2_{bias} \end{bmatrix} \tag{3.4}$$

The change to use both converted measurements and non-linear measurement equations results in a significantly different measurement vector, measurement mapping matrix and measurement covariance matrix.

$$\mathbf{z}(\mathbf{k}) = \begin{bmatrix} r(k)cos(\phi(k)) \\ r(k)sin(\phi(k)) \\ s^w(k) \\ \psi(k) \end{bmatrix} \tag{3.5}$$

$$\mathbf{h}(\mathbf{k}) = \begin{bmatrix} e_w(k) \\ n_w(k) \\ b\sqrt{\dot{e}_w^2(k) + \dot{n}_w^2(k)} \\ atan2(\dot{n}_{w_k}, \dot{e}_{w_k}) \end{bmatrix} \tag{3.6}$$

$$\mathbf{H}(\mathbf{k}) = \begin{bmatrix} 1 & 0 & 0 & 0 & 0 & 0 & 0 \\ 0 & 0 & 1 & 0 & 0 & 0 & 0 \\ 0 & \frac{b(k)\dot{e}_w(k)}{\sqrt{\dot{e}_w^2(k)+\dot{n}_w^2(k)}} & 0 & \frac{b(k)\dot{n}_w(k)}{\sqrt{\dot{e}_w^2(k)+\dot{n}_w^2(k)}} & 0 & 0 & 1 \\ 0 & \frac{-\dot{n}_w(k)}{\dot{e}_w^2(k)+\dot{n}_w^2(k)} & 0 & \frac{1}{\dot{e}_w(k)+\frac{\dot{n}_w^2(k)}{\dot{e}_w(k)}} & 0 & 0 & 0 \end{bmatrix} \tag{3.7}$$

$$\boldsymbol{\mu(k)} = \begin{bmatrix} r(k)cos(\phi(k))(e^{\sigma_\phi^2/2} - 1) \\ r(k)sin(\phi(k))(e^{\sigma_\phi^2/2} - 1) \\ 0 \\ 0 \end{bmatrix} \tag{3.8}$$

$$\begin{aligned} R_t^{11} =& r^2 e^{-\sigma_\phi^2}[cos^2(\phi)(cosh(\sigma_\phi^2) - 1) + sin^2(\phi)sinh(\sigma_\phi^2)] \\ &+ (\sigma_r^2 e^{-\sigma_r^2})[cos^2(\phi)cosh(\sigma_\phi^2) + sin^2(\phi) * sinh(\sigma_\phi^2)] \end{aligned} \tag{3.9a}$$

$$\begin{aligned} R_t^{22} =& r^2 e^{-\sigma_\phi^2}[sin^2(\phi)(cosh(\sigma_\phi^2) - 1) + cos^2(\phi)sinh(\sigma_\phi^2)] \\ &+ (\sigma_r^2 e^{-\sigma_r^2})[sin^2(\phi)cosh(\sigma_\phi^2) + cos^2(\phi) * sinh(\sigma_\phi^2)] \end{aligned} \tag{3.9b}$$

$$R_t^{12} = R_t^{21} = sin(\phi)cos(\phi)e^{-2\sigma_r^2}[\sigma_r^2 + r^2(1 - e^{\sigma_\phi^2})] \tag{3.9c}$$

$$R_t^{33} = \sigma_{s^w}^2 \tag{3.9d}$$

$$R_t^{44} = \sigma_\psi^2 \tag{3.9e}$$

At the start of the simulation, the bias ratio in the state vector is initialized with a

value of 1 to represent no prior knowledge of the presence of a bias. Prior to the turn, the filter is able to correctly resolve position, however, the current velocities and the bias cannot be adequately estimated without a second leg of data. In Figure 3-12a, the value of the NEES increases as the error between the estimated state and the actual state increases due to the the inaccurate estimation of the current and water referenced velocities. Figure 3-12b shows the bias present in the velocity components of the state vector with standard deviations at or outside of the 95% confidence bands. Additionally, Figure 3-10c reveals that the filter underestimates the bias present in the speed measurement. At the turn, the value of the NEES is significantly greater than the 99% confidence bound, indicating the filter is optimistic. After the turn, where the current magnitude and direction remain the same, but the water referenced velocity changes direction, the filter can now better distinguish error due to speed bias and the proper value of the current vector. Approximately 500 seconds after the turn, the bias estimation stabilizes at a value of 1.21 which compares favorably with the actual value of 1.20. With the correct estimation of the bias, the values of the estimated current velocities also approach their actual values as shown in Figure 3-10b. As the error in the state vector decreases, the NEES decreases as well until the filter is consistent by the end of the simulation. As with the previous simulations, the norm of the error covariance matrix and the NIS remain consistent throughout the run. In conclusion, this simulation demonstrated the ability of the filter to resolve reasonable values for the current velocities and the bias ratio. In this case, the geometry of two reciprocal track lines represents the best case scenario as a constant error magnitude will average to zero when applied in opposite directions. In the next chapter, the filter is modified for use with field data and the results analyzed.

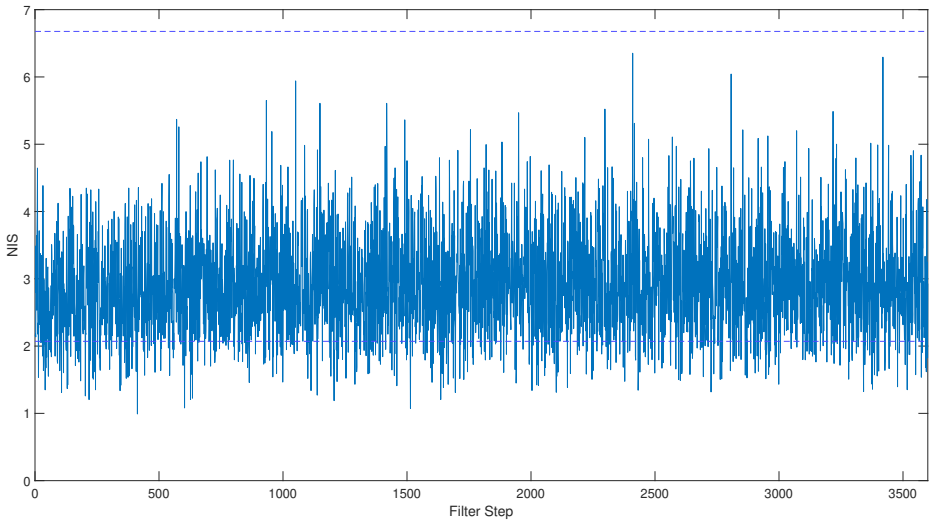

Figure 3-9: Innovation vector statistic with constant current, a 0.1 m/s speed bias and bias estimation. The NIS demonstrates the innovation vector is consistent throughout the simulation, which does not show the expected improvement in filter performance as a reasonable bias ratio is determined.

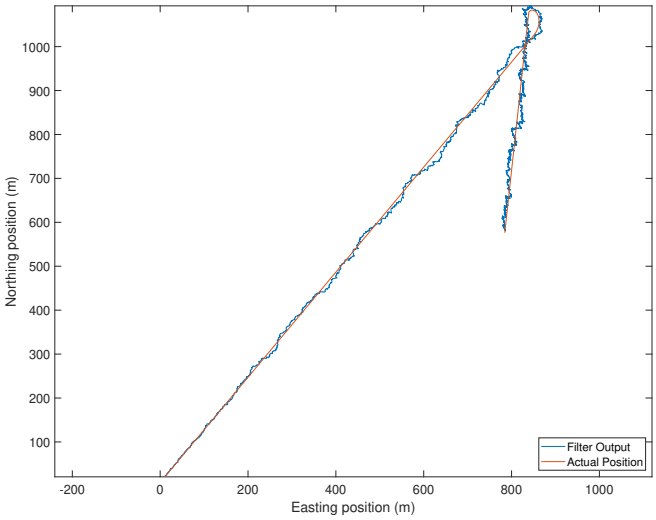

(a) Actual vs Filter Output Position

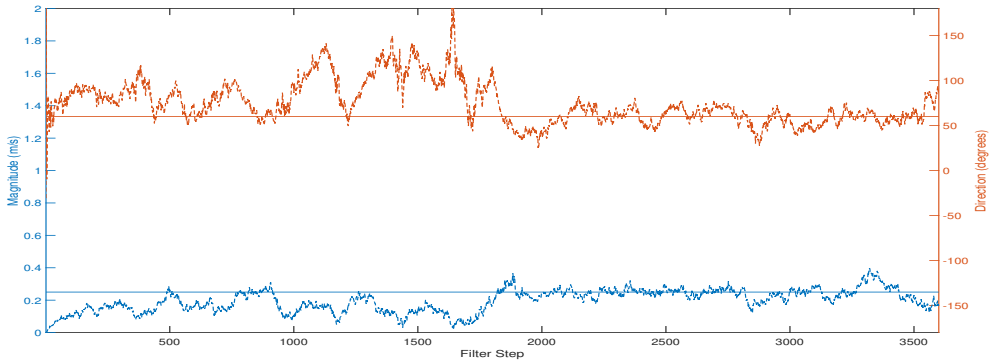

(b) Calculated Current Magnitude and Direction vs Filter Step

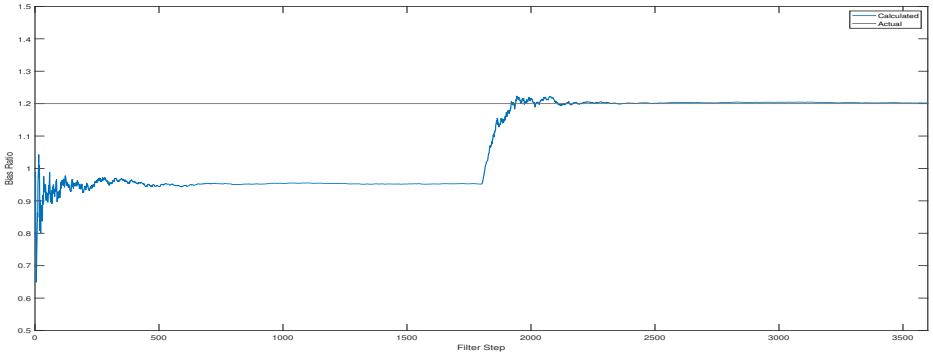

(c) Bias Ratio

Figure 3-10: Filter outputs of position and current magnitude and direction with constant current, a 0.1 m/s speed bias and bias estimation. The estimation of the current magnitude and direction does not agree well with the true values until after the turn when a reasonable bias ratio is determined.

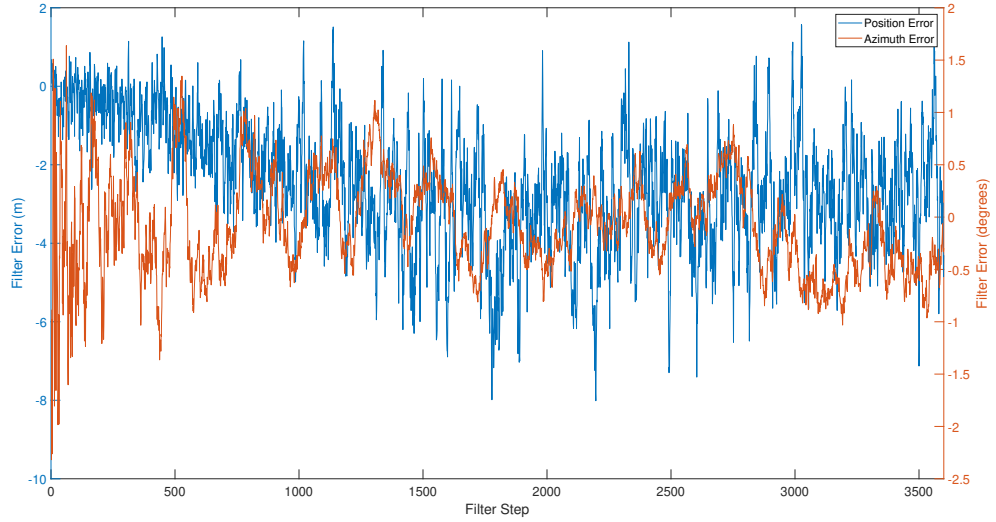

(a) Filter Error vs Filter Step

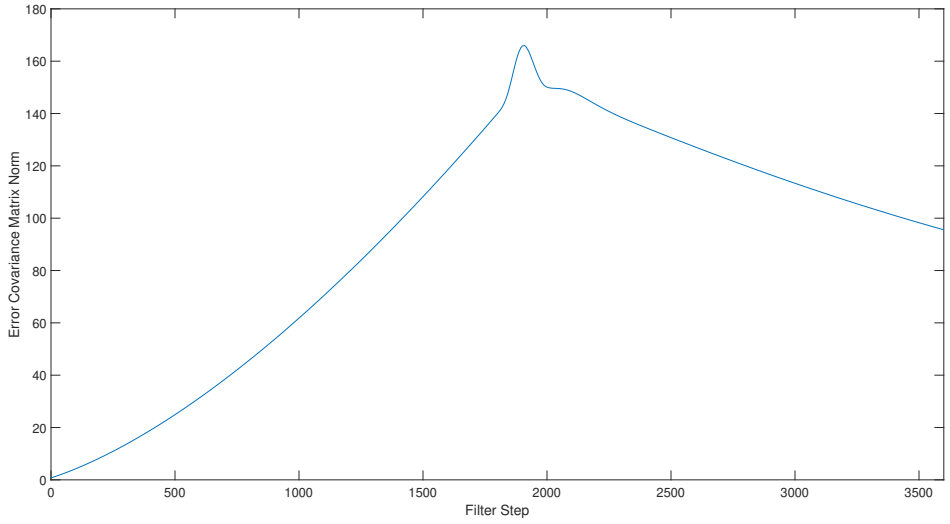

(b) Process Error Covariance Norm vs Filter Step

Figure 3-11: Filter error versus filter step and process noise covariance matrix norm with constant current, a 0.1 m/s speed bias and bias estimation. The simulation continues to show the range dependent characteristics of the range error and the value of the norm.

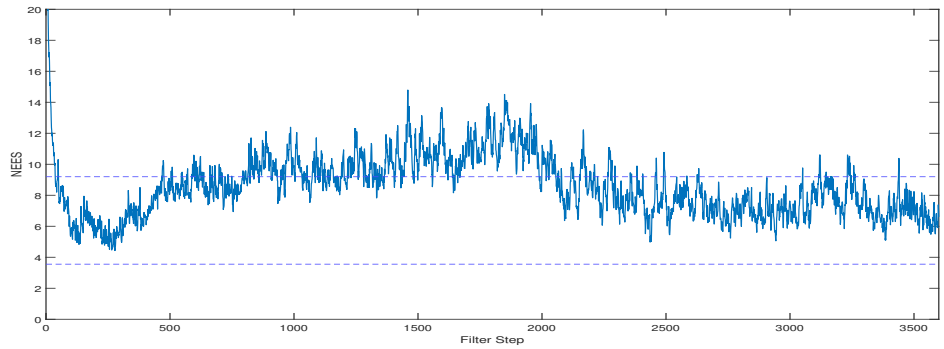

(a) 10 Run Normalized Estimation Error Squared (NEES)

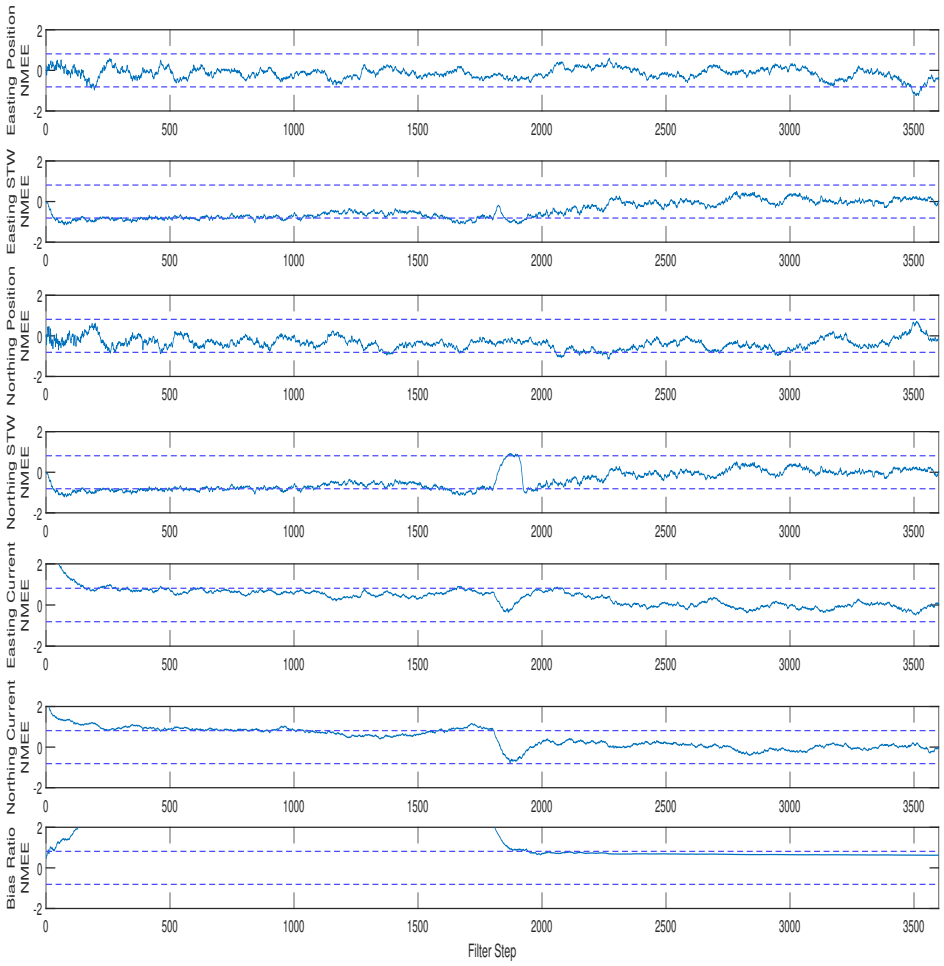

(b) Normalized Mean Estimation Error (NMEE)

Figure 3-12: State vector statistics with constant current, a 0.1 m/s speed bias and bias estimation. Prior to the turn, the bias causes the filter to be optimistic and the values of the NMEE for the bias and the velocities in the state vector are at or above the 95% confidence bounds. Once the turn is completed, the bias converges to a reasonable value and the filter becomes consistent as demonstrated by the values of both the NEES and the NMEE plotting inside their respective confidence bounds.

Chapter 4

Experimental Implementation

4.1 Vehicles and Sensors

To evaluate the filter's ability to process real data, a data set previously collected by Rypkema in support of [10] was chosen. The experiment, conducted on the Charles River at the Massachusetts Institute of Technology (MIT) Sailing Pavilion on September 14$^{\text{th}}$ 2018 included a Bluefin Robotics SandShark AUV, a small motorboat with the USBL sound source and a two element LBL system to provide position fixes for comparison to the navigation systems on the AUV.

Figure 4-1: Bluefin Robotics SandShark AUV fitted with a five element USBL acoustic receiving array providing input for calculations of range and angle from the source.

The navigation and control system on the AUV consists of two main subsystems, the main vehicle computer and the payload computer, connected by MOOS-iVP middleware. In

this design, the main vehicle computer provides navigational inputs to the payload section which processes the information and returns heading, speed, and depth commands to the main vehicle computer. The main vehicle computer then manipulates the control surfaces to match the vehicle motion to the requested input [2]. In addition to the main vehicle computer, the rear half of the unit also houses the AHRS, a depth sensor, a GPS, control surfaces and propulsion. The payload section in the forward half of the unit also contains the five element USBL receiving array, the chip scale atomic clock and a data acquisition system.

As well as a sound source, the motorboat was equipped with a GPS unit for precision measurement of the source location.

Two beacons mounted on the dock provided concurrent signals which were processed by the USBL system and used to determine the range from the sources. This passive LBL processing provides accurate range estimates for comparison to the output of any filter.

Further details about the vehicles and sensors can be found in [10].

4.2 Data and Data Processing

The LBL data was recorded in x and y coordinates referenced to a local origin. The USBL data was reported as range and angle from the source and when combined with the source location, provides a local reference frame position for the AUV. After the matched filter in the USBL processing algorithm calculates the maximum amplitude at each array element, the validity of the data is checked by comparing the sample number at which the maximum amplitude occurred. If the standard deviation of the sample number is greater than a pre-determined value, then the amplitudes cannot be assumed to be from the same source or the signal was distorted and the data is deemed unacceptable and reported as not-a-number (NaN) in the data table for that time. If the data is acceptable, the range and angle are calculated by combining the outputs of each array element[10].

Both the LBL and USBL data demonstrate noisy characteristics with many outlying data points. The EKF is designed to handle noisy data when the proper covariance values are used, but outlying data tends to significantly disrupt the output of the filter because the outliers occur much more often than a Gaussian distribution fit to the inlier data would predict. Prior to use in the filter, both the LBL and USBL data sets were manually curated

to remove the most egregious outliers. If this process were moved onto a fielded system, the curation would be automated via an outlier rejection algorithm. However, as the focus of this thesis is on current estimation and bias correction, manual curation was used to simplify analysis as though such a rejection algorithm were in place. As shown in Figure 4-2, The performance of the LBL data is significantly more consistent than the USBL data. Through the manual curation process, the majority of the erroneous LBL data was removed, creating a noisy, but mostly consistent pattern to the fixes. With the USBL data, the inconsistent fixes were not able to be completely removed and maintain sufficient information for the function of the filter. This resulted in requiring larger covariance values for range and angle to match the statistics of the filter to the real data at the expense of more noise in the filter output.

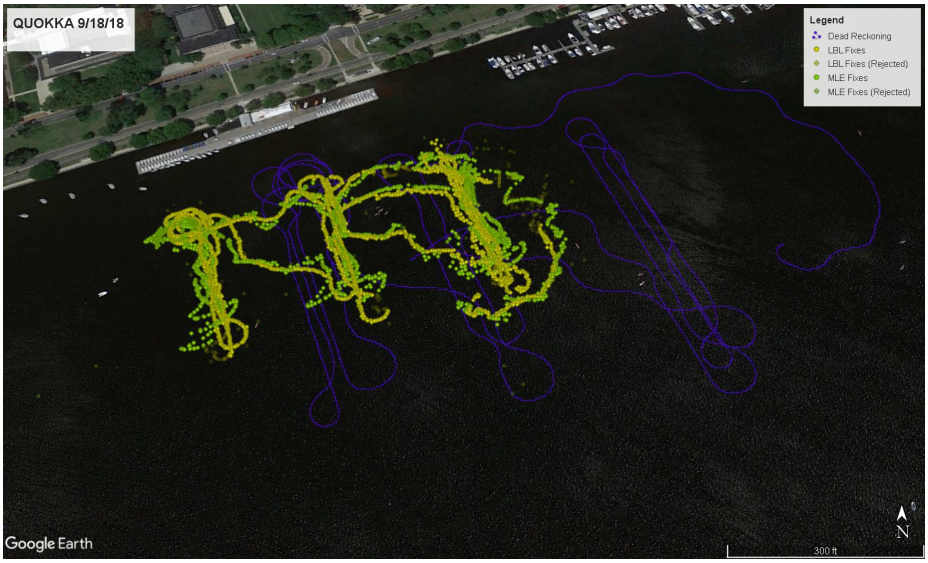

Figure 4-2: Geographic plot of the LBL fixes, USBL fixes and the DR solution from the main vehicle computer. Note the large difference in position calculation between the LBL fixes and the DR solution due to the biased speed reported by the main vehicle computer.

To minimize the adverse effects of excessively noisy data on the filter output, the functionality of the measurement specific correntropy filter as described by Fakoorian et al [4] was incorporated into the EKF. This technique applies a matrix gain determined using the measurement covariance matrix and the innovation vector to the calculation of the Kalman gain matrix in order to minimize the effect of outlying data. This gain matrix will reduce the weight of measurements that cause a large innovation which in turn reduces the disturbance on the filter calculated output. The gain matrix calculation and the change to the Kalman

gain matrix calculation result in the following equations:

$$\boldsymbol{C(k)} = \begin{bmatrix} \frac{e^{-R_{11}^{-1}} r_1(k)^2}{2\sigma^2(k)} & 0 & 0 & 0 \\ 0 & \frac{e^{-R_{22}^{-1}} r_2(k)^2}{2\sigma^2(k)} & 0 & 0 \\ 0 & 0 & \frac{e^{-R_{33}^{-1}} r_3(k)^2}{2\sigma^2(k)} & 0 \\ 0 & 0 & 0 & \frac{e^{-R_{44}^{-1}} r_4(k)^2}{2\sigma^2(k)} \end{bmatrix} \tag{4.1}$$

$$\mathbf{W(k+1)} = (\mathbf{P(k+1|k)^{-1}} + \mathbf{H(k+1)'C(k)R^{-1}H(k+1)})^{-1} + \mathbf{H(k+1)'C(k)R^{-1}} \tag{4.2}$$

In addition to the LBL and USBL acoustic fixes, the data set includes the DR solution from the navigation system operating on the main vehicle computer. This solution was generated using heading from the AHRS and the propeller RPM with a pre-determined calibration equation to determine vehicle speed. As discussed in Chapter 3, the calibration equation was generated by Bluefin Robotics using a smooth unmodified hull, and is not representative of the current configuration. The effect of the speed bias is seen in Figure 4-2 as the dead reckoned solution legs are significantly longer than those determined from the more accurate passive LBL data.

4.3 Filter Variants

In this section, five filter configurations which process the available data in different ways will be described in terms of function and value. The filter or combination of filters used is determined by whether or not updated and valid acoustic data is available as well as the source of the acoustic data.

In this experiment, the main vehicle computer navigation system reports the speed and heading at 10 Hz while the acoustic measurements are reported at approximately 1 Hz. In order to maximize sensitivity to changes in speed or heading by processing all available navigation data, the filter developed operates at 10 Hz. Additionally, some of the acoustic data was deemed invalid by the USBL processing, and the filter must also be able to handle those instances. Because of this, a filter was developed that only uses speed and heading from the main vehicle computer as inputs. This allows the state vector to evolve by DR during the cycles between valid acoustic measurements.

In order to provide a baseline current velocity estimation for comparison, a filter using

the LBL data was developed. Because the data is recorded as local x and y coordinates vice range and angle, the filter required modification.

When valid acoustic data is available, one filter estimates the state using both the range and angle data. While the data conforms to the assumptions of the state transition model, the use of all available data will produce the most robust state estimate.

However, as described in [10], the standard deviation of the angle measurements was significantly higher than that of the range measurements. The variability of the angle causes the track developed by the USBL data to diverge considerably from the LBL fixes. To combat this, a filter using only range data was developed.

Finally, analysis of the range/angle and range only filters showed that each outperformed the other in different situations. To select the best state estimate at a given time step, both filters are run in parallel and a method to chose the most likely output was developed.

4.3.1 Acoustic Measurements Unavailable

During the times in between acoustic measurements, or if the acoustic measurement data is deemed inconsistent, the filter will use the speed and heading inputs only in the measurement vector. As a result, the stochastic parameters, measurement vector, mapping matrix and covariance matrix were changed to the following:

Table 4.1: Standard Deviations of Various Variables when Acoustic Data Unavailable

Parameter	Value
$\sigma_{position}$	1.0 m
$\sigma_{velocity}$	0.5 m/s
$\sigma_{current}$	0.05 m/s
σ_{bias}	0.001 m/s
σ_{s^w}	1 m/s
σ_{ψ}	2 deg

$$\mathbf{z}(\mathbf{k}) = \begin{bmatrix} s^w(k) \\ \psi(k) \end{bmatrix} \tag{4.3}$$

$$\mathbf{h}(\mathbf{k}) = \begin{bmatrix} b\sqrt{\dot{e}_w^2(k) + \dot{n}_w^2(k)} \\ atan2(\dot{n}_{w_k}, \dot{e}_{w_k}) \end{bmatrix} \tag{4.4}$$

$$\mathbf{H} = \begin{bmatrix} 0 & \frac{b\dot{e}_w(k)}{\sqrt{\dot{e}_w^2(k)+\dot{n}_w^2(k)}} & 0 & \frac{b\dot{n}_w(k)}{\sqrt{\dot{e}_w^2(k)+\dot{n}_w^2(k)}} & 0 & 0 & 1 \\ 0 & \frac{-\dot{n}_w(k)}{\dot{e}_w^2(k)+\dot{n}_w^2(k)} & 0 & \frac{1}{\dot{e}_w(k)+\frac{\dot{n}_w^2(k)}{\dot{e}_w(k)}} & 0 & 0 & 0 \end{bmatrix} \tag{4.5}$$

$$\mathbf{R} = \begin{bmatrix} \sigma_{s^w}^2 & 0 \\ 0 & \sigma_{\psi}^2 \end{bmatrix} \tag{4.6}$$

Because this filter was only used in the absence of valid acoustic data, a full run was never conducted using only this filter.

4.3.2 Long Baseline (LBL) Measurements

While this data set does not include ADCP measurements to establish a baseline to compare to the filter output, the LBL position measurements will serve as the basis for comparison with current vectors estimated by the filter. LBL meassurements offer a higher accuracy than USBL due to the fact that the LBL system determines position from the intersection of range circles which do not exhibit a range dependent error as in the case of USBL. In this case, the LBL data is reported in local x and y coordinates vice range and angle, so no conversion from polar to Cartesian coordinates needs to take place in the filter. The resulting standard deviation values, measurement vector, measurement mapping matrix and covariance matrix are as follows:

Table 4.2: Standard Deviations of Various Variables Using LBL Data

Parameter	Value
$\sigma_{position}$	1.0 m
$\sigma_{velocity}$	0.5 m/s
$\sigma_{current}$	0.05 m/s
σ_{bias}	0.001 m/s
σ_r	10 m
σ_{s^w}	.5 m/s
σ_{ψ}	2 deg

$$\mathbf{z}(\mathbf{k}) = \begin{bmatrix} x_{LBL} \\ y_{LBL} \\ s^w(k) \\ \psi(k) \end{bmatrix} \tag{4.7}$$

$$\mathbf{H} = \begin{bmatrix} 1 & 0 & 0 & 0 & 0 & 0 & 0 \\ 0 & 0 & 1 & 0 & 0 & 0 & 0 \\ 0 & \frac{b\dot{e}_w(k)}{\sqrt{\dot{e}_w^2(k)+\dot{n}_w^2(k)}} & 0 & \frac{b\dot{n}_w(k)}{\sqrt{\dot{e}_w^2(k)+\dot{n}_w^2(k)}} & 0 & 0 & 1 \\ 0 & \frac{-\dot{n}_w(k)}{\dot{e}_w^2(k)+\dot{n}_w^2(k)} & 0 & \frac{1}{\dot{e}_w(k)+\frac{\dot{n}_w^2(k)}{\dot{e}_w(k)}} & 0 & 0 & 0 \end{bmatrix} \tag{4.8}$$

$$\mathbf{R} = \begin{bmatrix} \sigma^2_{position} & 0 & 0 & 0 \\ 0 & \sigma^2_{position} & 0 & 0 \\ 0 & 0 & \sigma^2_{s^w} & 0 \\ 0 & 0 & 0 & \sigma^2_{\psi} \end{bmatrix} \tag{4.9}$$

4.3.3 Ultra-short Baseline (USBL) Range and Angle Measurements

With field data, the ground truth is unknown and the covariance calculations are modified to use the measured data. This process, which involves determining the average true bias and average true covariance is described in [8]. Additionally, the simulations were conducted with ranges relative to a stationary source while for this experiment, the source was moving. This requires the addition of the source position to the range and angle calculations of the measurement vector. For this filter, the resulting standard deviations, measurement vector, measurement bias and covariance matrix are as follows:

Table 4.3: Standard Deviations of Various Variables using USBL Range and Angle Data

Parameter	Value
$\sigma_{position}$	1 m
$\sigma_{velocity}$	0.5 m/s
$\sigma_{current}$	0.05 m/s
σ_{bias}	0.001 m/s
σ_r	30 m
σ_ϕ	10 deg
σ_{s^w}	1 m/s
σ_ψ	2 deg

$$\mathbf{z}(\mathbf{k}) = \begin{bmatrix} x_{source} - r(k)cos(\phi(k)) \\ y_{source} - r(k)sin(\phi(k)) \\ s^w(k) \\ \psi(k) \end{bmatrix} \tag{4.10}$$

$$\boldsymbol{\mu(k)} = \begin{bmatrix} r(k)cos(\phi(k))(e^{-\sigma_\phi^2} - e^{-\sigma_\phi^2/2}) \\ r(k)sin(\phi(k))(e^{-\sigma_\phi^2} - e^{-\sigma_\phi^2/2}) \\ 0 \\ 0 \end{bmatrix} \tag{4.11}$$

$$\begin{aligned} R_t^{11} =& r^2 e^{-2\sigma_\phi^2}[cos^2(\phi)(cosh(2\sigma_\phi^2) - cosh(\sigma_\phi^2)) + sin^2(\phi)(sinh(2\sigma_\phi^2) - sinh(\sigma_\phi^2))] \\ &+ (\sigma_r^2 e^{-2\sigma_r^2})[cos^2(\phi)(2cosh(2\sigma_\phi^2) - cosh(\sigma_\phi^2)) + sin^2(\phi)(2sinh(2\sigma_\phi^2) - sinh(\sigma_\phi^2))] \end{aligned} \tag{4.12a}$$

$$\begin{aligned} R_t^{22} =& r^2 e^{-2\sigma_\phi^2}[sin^2(\phi)(cosh(2\sigma_\phi^2) - cosh(\sigma_\phi^2)) + cos^2(\phi)(sinh(2\sigma_\phi^2) - sinh(\sigma_\phi^2))] \\ &+ (\sigma_r^2 e^{-2\sigma_r^2})[sin^2(\phi)(2cosh(2\sigma_\phi^2) - cosh(\sigma_\phi^2)) + cos^2(\phi)(2sinh(2\sigma_\phi^2) - sinh(\sigma_\phi^2))] \end{aligned} \tag{4.12b}$$

$$R_t^{12} = R_t^{21} = sin(\phi)cos(\phi)e^{-4\sigma_r^2}[\sigma_r^2 + (r^2 + \sigma_r^2)(1 - e^{\sigma_\phi^2})] \tag{4.12c}$$

$$R_t^{33} = \sigma_{s^w}^2 \tag{4.12d}$$

$$R_t^{44} = \sigma_\psi^2 \tag{4.12e}$$

4.3.4 USBL Range Only Measurements

As discussed in [10], a review of the USBL data set revealed that the standard deviation of the angle measurements was considerably larger than that of the range measurements, especially in turns. This effect is believed to be due to a bias induced by an interaction between the incoming acoustic signal and the hull of the AUV and is geometry-dependent. While the USBL processing uses a method to compensate for the bias, the structure of the angle measurements as shown in Figure 4-2 does not conform to a Gaussian distribution and will cause problems with a filter that assumes the noise is Gaussian distributed. In order to further minimize these effects, a filter variant using only the range input was produced and tested. These changes resulted in the following standard deviations, measurement vectors,

measurement mapping matrix, and measurement covariance matrix:

Table 4.4: Standard Deviations of Various Variables using USBL Range Only Data

Parameter	Value
$\sigma_{position}$	1 m
$\sigma_{velocity}$	0.5 m/s
$\sigma_{current}$	0.05 m/s
σ_{bias}	0.001 m/s
σ_r	10 m
σ_{s^w}	.5 m/s
σ_ψ	2 deg

$$\mathbf{z}(\mathbf{k}) = \begin{bmatrix} r(k) \\ s^w(k) \\ \psi(k) \end{bmatrix} \tag{4.13}$$

$$\mathbf{h}(\mathbf{k}) = \begin{bmatrix} \sqrt{e_g^2(k) + n_g^2(k)} \\ b\sqrt{\dot{e}_w^2(k) + \dot{n}_w^2(k)} \\ atan2(\dot{n}_{w_k}, \dot{e}_{w_k}) \end{bmatrix} \tag{4.14}$$

$$\mathbf{H}(\mathbf{k}) = \begin{bmatrix} 1 & 0 & 0 & 0 & 0 & 0 & 0 \\ 0 & \frac{b\dot{e}_w(k)}{\sqrt{\dot{e}_w^2(k)+\dot{n}_w^2(k)}} & 0 & \frac{b\dot{n}_w(k)}{\sqrt{\dot{e}_w^2(k)+\dot{n}_w^2(k)}} & 0 & 0 & 1 \\ 0 & \frac{-\dot{n}_w(k)}{\dot{e}_w^2(k)+\dot{n}_w^2(k)} & 0 & \frac{1}{\dot{e}_w(k)+\frac{\dot{n}_w^2(k)}{\dot{e}_w(k)}} & 0 & 0 & 0 \end{bmatrix} \tag{4.15}$$

$$\mathbf{R} = \begin{bmatrix} \sigma_{range}^2 & 0 & 0 \\ 0 & \sigma_{s^w}^2 & 0 \\ 0 & 0 & \sigma_\psi^2 \end{bmatrix} \tag{4.16}$$

4.3.5 Parallel USBL Processing

Analysis of the previous two filters revealed that each performed better than the other at certain times during the data set. To maximize the accuracy of the filter output, a parallel filter structure was developed. This method processes the valid USBL acoustic data using both the range/angle filter and the range only filter. After both functions have computed an output, the norm of the innovation vector of each filter at the current step is compared and

the filter with the smallest norm is chosen as the best estimate. Once a filter is chosen, the state estimate vector becomes the output of the main filter process and the state estimate vector, along with the process noise covariance matrix, become the input for both filters on subsequent steps.

Table 4.5: Standard Deviations of Various Variables using Parallel USBL Processing

Parameter	Value
$\sigma_{position}$	1 m
$\sigma_{velocity}$	0.5 m/s
$\sigma_{current}$	0.05 m/s
σ_{bias}	0.001 m/s
$\sigma_{r_{range\ and\ angle}}$	10 m
$\sigma_{r_{range\ only}}$	30 m
σ_{ϕ}	6 deg
σ_{s^w}	1 m/s
σ_{ψ}	2 deg

4.4 Experimental Results

4.4.1 LBL Measurements

Beginning in the vicinity of (48,-72), the AUV proceeds to the east and conducts multiple legs perpendicular to the shore. In simulation, legs with reciprocal courses were determined to offer the most useful data. After completion of the easternmost legs, the pattern is repeated in two additional locations to the west. Once the racetrack legs are completed, the AUV then transits northeast parallel to the shore before turning in a wide arc to finish the run south of the easternmost racetrack leg. In Figure 4-3a, the filter output is shown in blue with the LBL position fixes used as the input to the filter plotted in red. After removing outliers, the consistent LBL data results in a consistent and accurate position output from the filter. Of note, the two relatively long sections near the end of the run that do not have LBL data demonstrate the position drift inherent in a DR process and also the filter's ability to correct the position output when consistent data is once again available.

As with the simulation runs, the bias element of the state vector is initialized with a value of 1 to represent no prior knowledge of the existence of a bias. Figure 4-3b shows that

as the filter processes data from successive legs, the bias appears to converge asymptotically to an approximate value of 1.67. This indicates that the speed reported from the main vehicle computer is 1.67 times the actual value.

In Figure 4-3c, the effect of the changing bias can be seen in the plots of both the magnitude and the direction. As the bias increases, the magnitude of the current decreases to a value near 0.1 m/s and the direction in the vicinity of 200-250 degrees. This compares favorably with the expectation of a direction near to parallel with the shore and a small magnitude in a section of river upstream of a dam. The effects of the turns and inconsistent data can also be seen in the direction as the output wraps around 0 and 360 to converge on approximately the same value for the next steady leg.

Although the value of the bias ratio appeared to converge to a steady value, the short duration of the data set leaves the actual final value in question. To determine if the filter would calculate a different final value of the bias ratio, the data was reprocessed with the bias component of the state vector initialised to 1.67. The resulting position output, plotted in Figure 4-4a, shows a similar performance as with the first processing with a slight decrease in the number and magnitude of outliers in the position calculation. In Figure 4-4b, the behavior is once again exponential with a asymptotic behavior, converging to a final value of 1.78. Unlike the first processing of the data, the bias ratio approached its final value in the first third of the run, indicating that this number is more likely to be representative of the true value of the bias than the 1.67 first determined. Because the filter was initialized with a bias ratio closer to the true value, the current magnitude and direction are more realistic at the beginning of the run and are slowly refined as the bias ratio is slightly increased.

4.4.2 USBL Range and Angle Measurements

As previously discussed, the standard deviation of the USBL data was larger than that of the LBL data, and this inconsistency shows in the plot of USBL fixes in Figure 4-5a. The filter position output adequately follows the USBL input, but the output does not agree well with the LBL fixes because of the less accurate input. In order to make the inconsistent angle measurements have less of an effect on the output, the covariance can be increased, however, increasing the covariance to the point that the the inconsistent data does not affect the output effectively forces the filter to ignore the angle measurements altogether. Additionally, the increased covariance lowers the filter gain, placing more weight on the

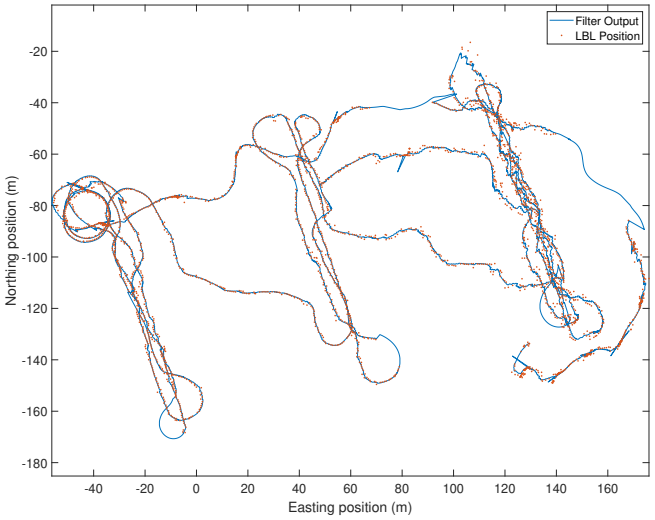

(a) Filter Output With LBL Inputs

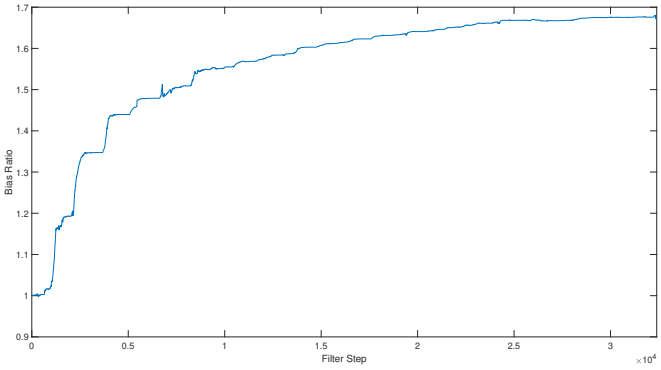

(b) Calculated Bias with LBL Inputs

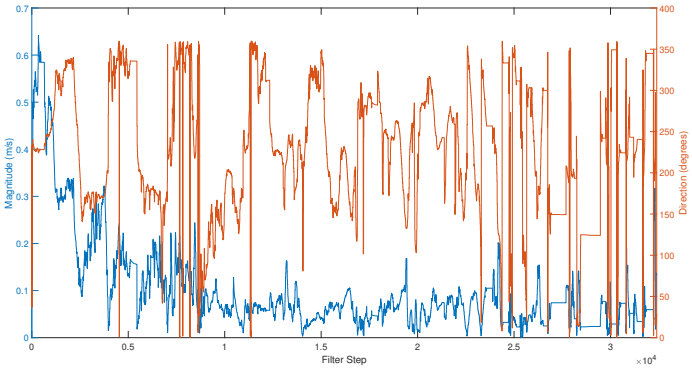

(c) Calculated Current Magnitude and Direction with LBL Inputs

Figure 4-3: LBL processing with bias initialized at 1, indicating no prior knowledge of a bias present. Note that as the bias increases, the magnitude and direction of the calculated current converge on reasonable values.

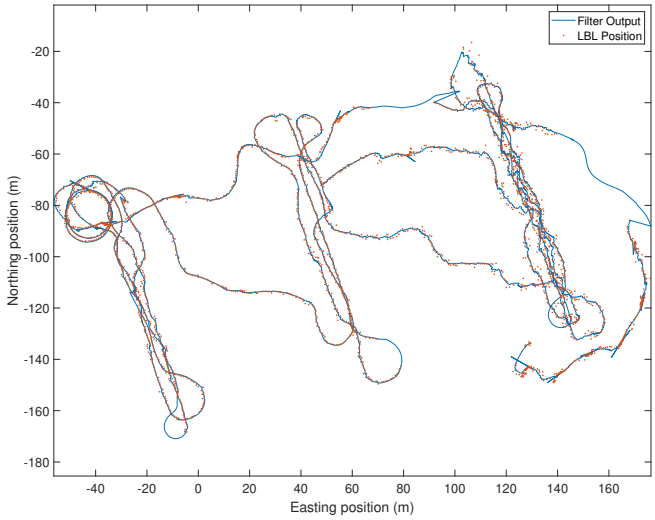

(a) Filter Output With LBL Inputs and Calculated Bias

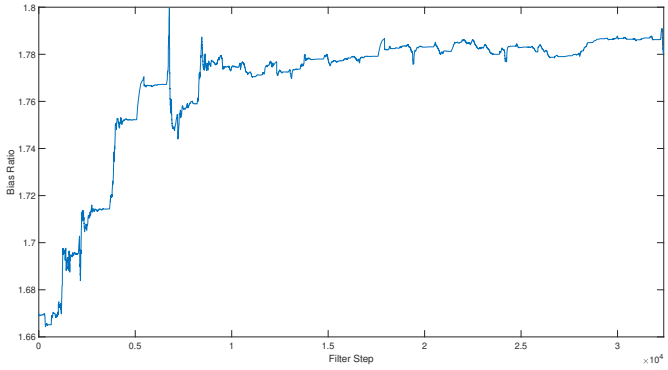

(b) Calculated Bias with LBL Inputs and Calculated Bias

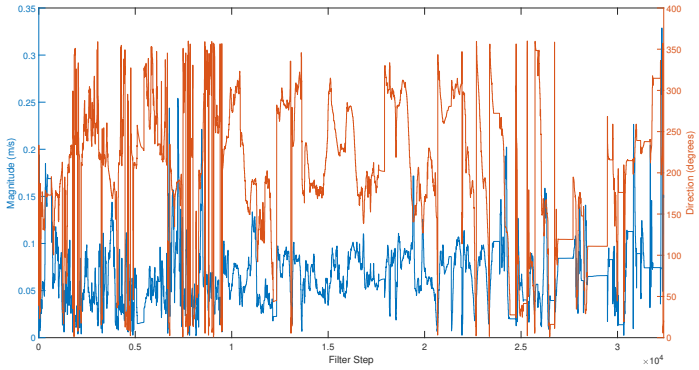

(c) Calculated Current Magnitude and Direction with LBL Inputs and Calculated Bias

Figure 4-4: LBL processing using an initial bias value of 1.67. With the filter initialized with a reasonable bias value, the estimated state values reach a consistent value much earlier in the run than the previous case.

present state estimation which is initially inaccurate as the filter is initialized with no prior knowledge of the current velocity or bias. For these reasons, a separate range only filter was developed as described above. Similar to the LBL filter, the plot of the bias ratio shown in Figure 4-5b increases exponentially from the initial value of 1 to asymptotically approach a steady value, which in this case is 1.75. As the bias ratio increases, the magnitude and direction of the calculated current plotted in Figure 4-5c settle on values that are consistent on each steady leg. In comparison to the LBL filter, the effects of the turns is similar, however, the effect of inconsistent data, especially near the end of the run, are more pronounced. At approximately 2300 seconds, corresponding with positions in the northeast corner of the position plot, the data demonstrates a large variance for an unknown reason and many outliers were removed from this area. This increased variance and sparse data contributes to an inaccurate estimation current direction. Once consistent data is again obtained, the filter converges again toward a value between 200 and 250 degrees.

Figure 4-6a shows the position output of a second run of the filter with the bias ratio initialized with the final value from the first run. Compared to the previous USBL range and angle position output, the results are very similar with no substantial differences. The bias ratio in Figure 4-6b demonstrates a slightly different behavior than the previous case. In this instance, the value rises to a maximum and then slowly lowers for the remainder of the run, ending at a value of 1.95. Comparing the calculation of the magnitude and direction of current from the first and second processing runs, both plots exhibit similar behavior with respect to turns and inconsistent data, however, the second run converges to a reasonable value of current more quickly.

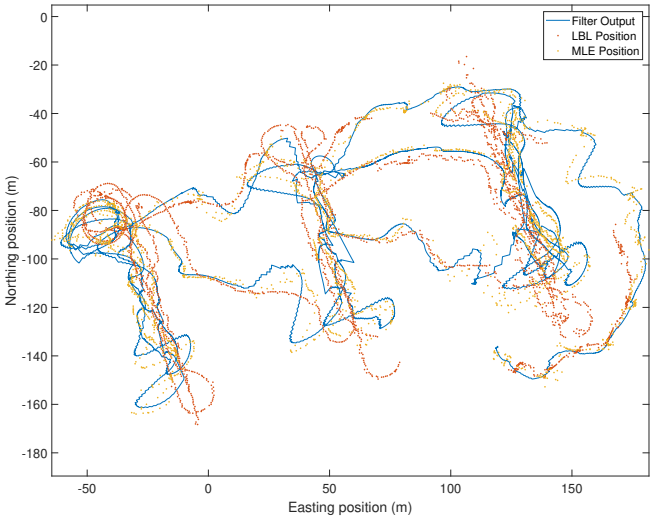

(a) Filter Output With USBL Range and Angle Inputs

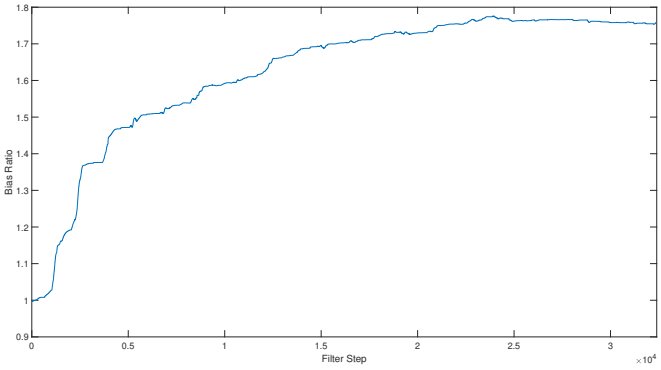

(b) Calculated Bias with USBL Range and Angle Inputs

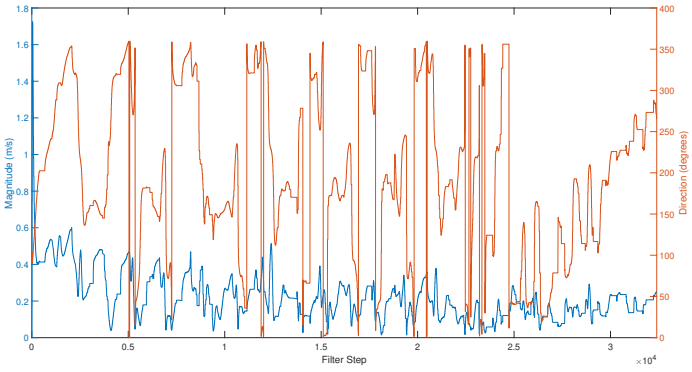

(c) Calculated Current Magnitude and Direction with USBL Range and Angle Inputs

Figure 4-5: USBL range and angle processing using an initial bias value of 1. The inconsistency of the data, especially the angle measurements, results in the filter output deviating significantly from the LBL fixes.

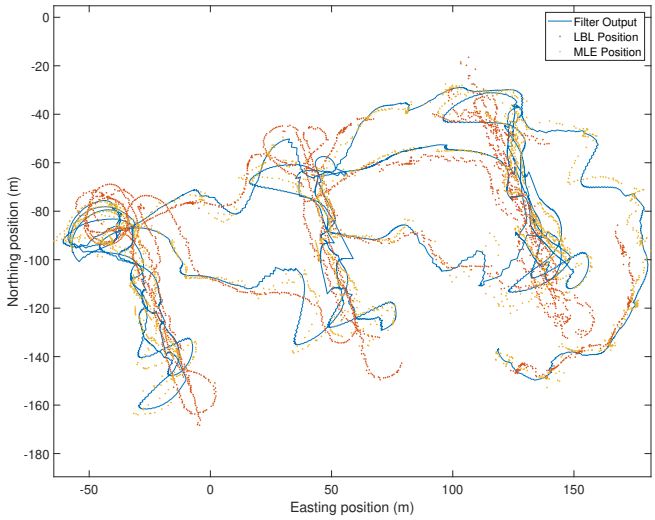

(a) Filter Output With USBL Range and Angle Inputs and Calculated Bias

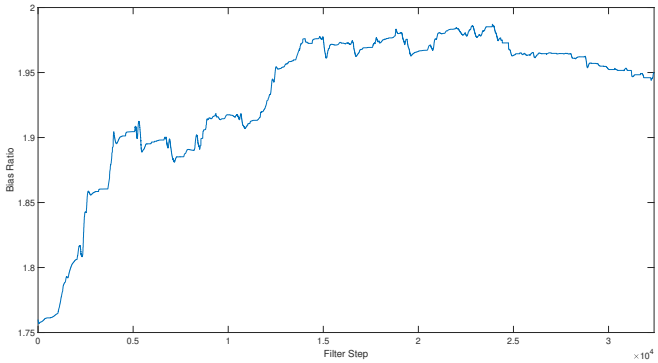

(b) Calculated Bias with USBL Range and Angle Inputs and Calculated Bias

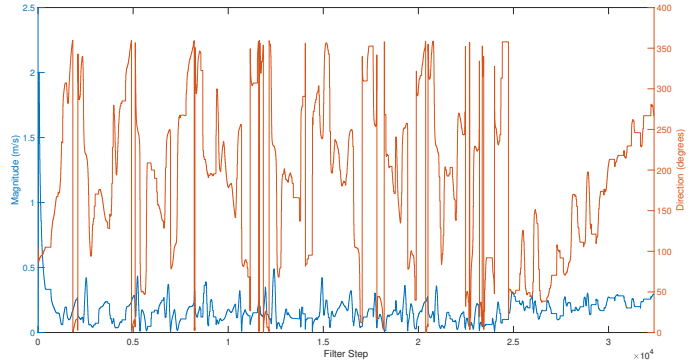

(c) Calculated Current Magnitude and Direction with USBL Range and Angle Inputs and Calculated Bias

Figure 4-6: USBL range and angle processing using an initial bias value of 1.75. While the calculated current and magnitude reach reasonable values more quickly than the first case, the position output still does not agree well with the LBL filter because of the inconsistent input data.

4.4.3 USBL Range Only Measurements

Using only the range measurements to calculate the position output results in significantly more accurate estimation in several locations along the track as compared to using both the range and angle data as shown in Figure 4-7a. On the legs crossing between the racetracks and on the arc in the northwest corner, the effect of the inconsistent angle measurements can be seen as the filter output is consistent with the LBL fixes and the raw fixes are not. Although some improvement was demonstrated, the calculated position does not agree well with the LBL fixes on the racetrack legs. Insight into why the calculated position disagrees on the racetrack legs where the data is most consistent is provided by the plot of the bias ratio in Figure 4-7b. The plot demonstrates similar behavior to the previous filters, however, the bias ratio approaches a much higher value of 2.54. This larger ratio causes the calculated water referenced speed to be erroneously low and the current velocities to be erratic. Figure 4-7c shows the effects of the incorrect bias ratio. Even with an accurate heading, the smaller magnitude of the water referenced velocity vector causes the current magnitude and calculated direction to be incorrect and inconsistent as well.

As with the previous filters, a second processing run was conducted with the bias component of the state vector initialized with the final bias ratio from the first run. In the first run, the higher than expected bias ratio cause position calculation errors and starting from a high ratio compounded the problem. The position output in Figure 4-8a displays considerable inconsistency and does not agree well with the LBL fixes. A review of Figure 4-8b shows the already high bias ratio of the second run continuing to increase, ending at a value of 3.1, nearly twice the reference value calculated by the LBL filter. The effect of this bias is illustrated in the inconsistent current magnitude and direction calculations in Figure 4-8c.

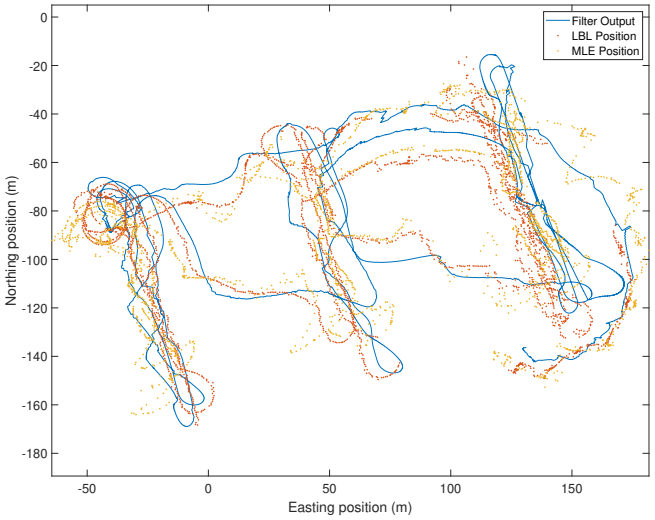

(a) Filter Output With USBL Range Only Inputs

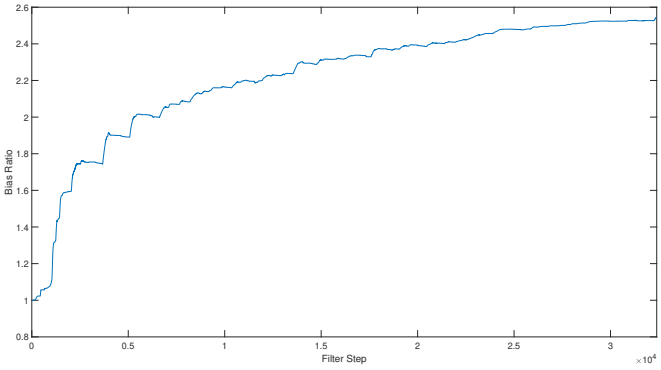

(b) Calculated Bias with USBL Range Inputs

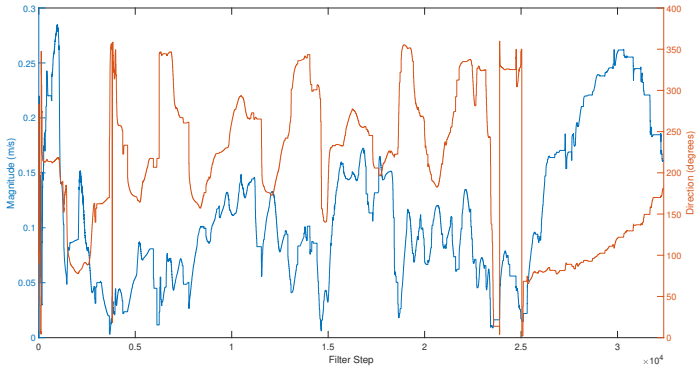

(c) Calculated Current Magnitude and Direction with USBL Range Inputs

Figure 4-7: USBL range only processing using an initial bias value of 1. Unlike the previous cases, the calculated bias increases above 2.0, causing an erroneous calculation of the water referenced speed and therefore the current velocities as well.

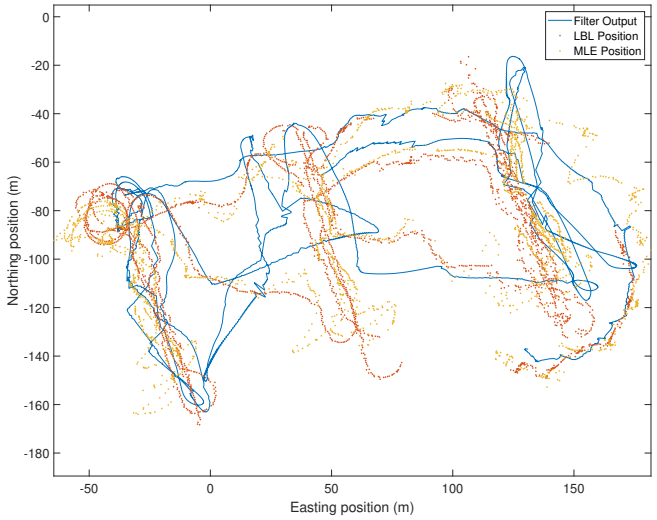

(a) Filter Output With USBL Range Inputs and Calculated Bias

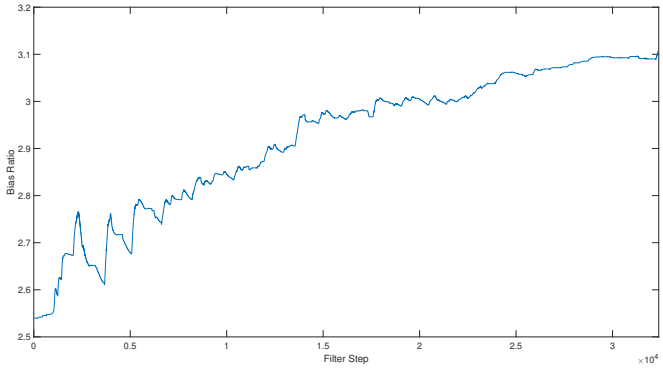

(b) Calculated Bias with USBL Range Inputs and Calculated Bias

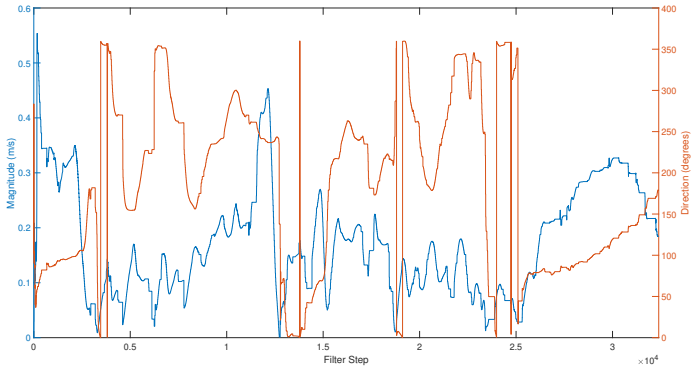

(c) Calculated Current Magnitude and Direction with USBL Range Inputs and Calculated Bias

Figure 4-8: USBL range only processing using an initial bias value of 2.54. The falsely high bias ratio now not only affects the consistency of the calculated current velocity, but also the position calculation.

4.4.4 Parallel USBL Processing

Operating both the USBL range/angle and range only filters in parallel offers the most accurate solution by choosing the best performing output at each filter step. The position output plotted in Figure 4-9a shows inconsistencies at the beginning of the run while the bias ratio is too low, but gains agreement with the LBL fixes during the second set of racetrack legs. The bias ratio shown in Figure 4-9c demonstrates the expected behavior and converges to a value of 1.66, which compares favorably to the first run of the LBL filter. Prior to the inconsistent USBL data at approximately 2500 seconds into the run, the behavior of the calculated current direction and magnitude is similar to the LBL filter. After the inconsistent data, the filter begins to converge again on the expected values of magnitude and direction.

For the second run, the position output shown in Figure 4-10a demonstrates high consistency and agreement with respect to the LBL fixes. Additionally, the bias ratio in Figure 4-10c again demonstrates the expected behavior with a final value of 1.8, which is also consistent with the second run of the LBL filter. Comparing the plots of current direction and magnitude from the second runs of the LBL and parallel filters shows similar behavior and values.

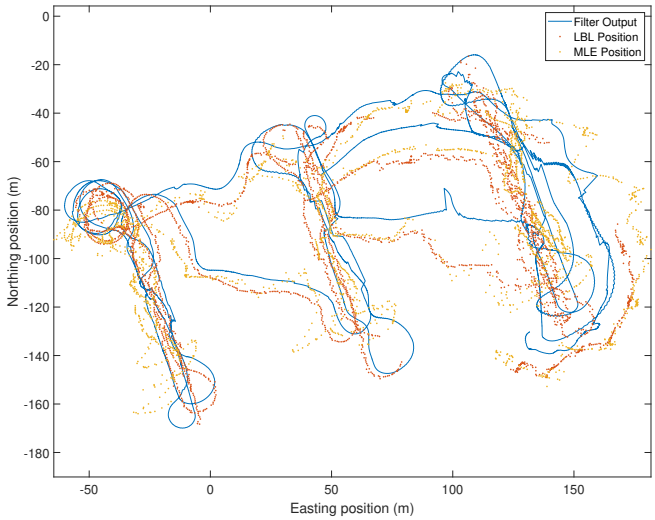

(a) Filter Output With Parallel USBL Processing

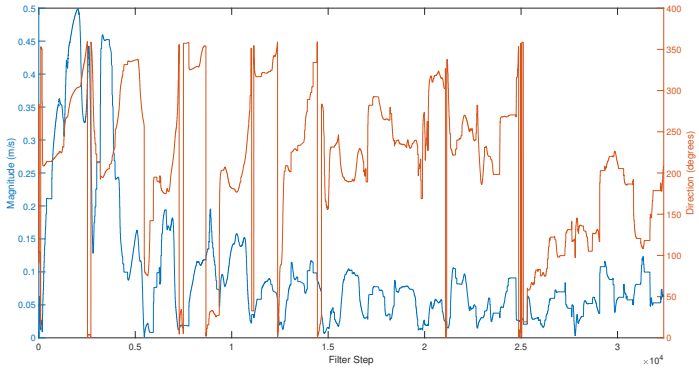

(b) Calculated Current Magnitude and Direction with Parallel USBL Processing

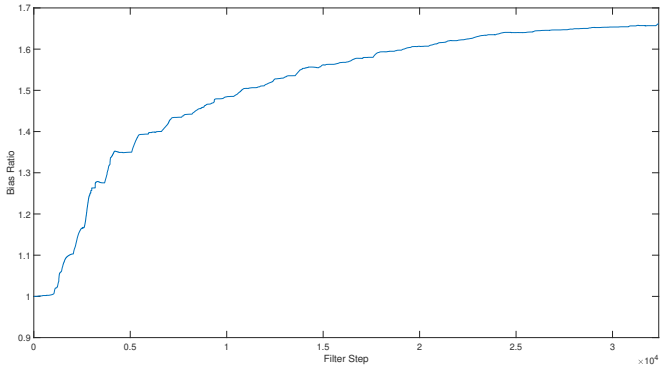

(c) Calculated Bias with Parallel USBL Processing

Figure 4-9: Parallel USBL processing using an initial bias value of 1. With no prior knowledge of bias, the filter is initially inconsistent. As the bias ratio approaches the final value, the position output and the calculations of current magnitude and direction begin to agree with the LBL filter.

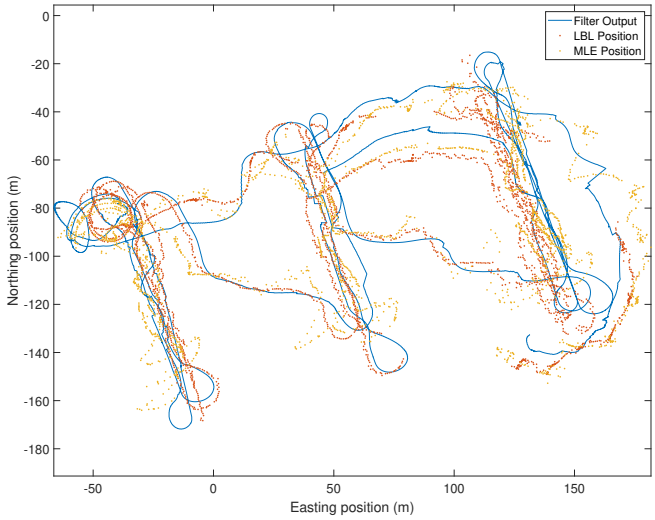

(a) Filter Position Output

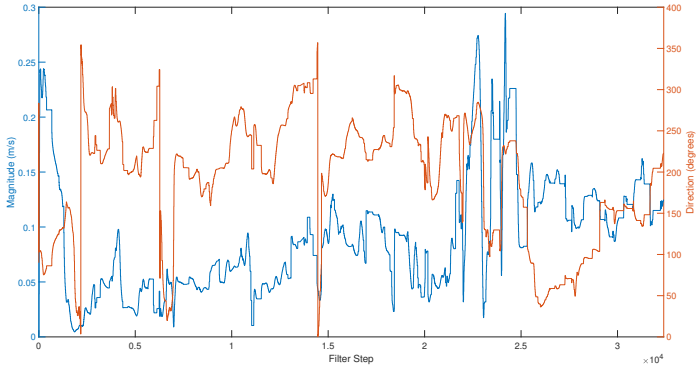

(b) Calculated Current Magnitude and Direction

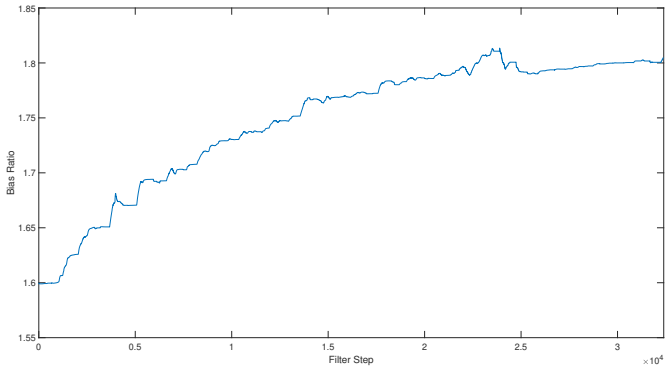

(c) Calculated Bias

Figure 4-10: Parallel USBL processing using an initial bias value of 1.66. With the filter initialized with a reasonable bias value, the estimated state values become consistent with the LBL filter much more quickly.

Chapter 5

Conclusion

5.1 Summary of Results

The main goal of this thesis research was to investigate if the velocity of the water current affecting vehicle motion could be calculated without the addition of a DVL or ADCP. The method proposed in this thesis demonstrates the effectiveness of a navigation solution for the calculation of current velocities using an acoustic navigation system in conjunction with DR navigation.

A system consisting of three EKFs uses a NCV model of kinetic motion along with combinations of range and angle measurements from a USBL acoustic navigation system and speed and heading measurements reported by the main vehicle computer to estimate the state of the system. This system state consists of the easting and northing components of the geographic coordinates in a local reference frame, the water-referenced vehicle velocity and the water current velocity as well as a bias ratio that describes the relation between the speed calculated by the main vehicle computer and the actual water-referenced speed. The output of the main process is determined by the available data and by comparing the innovation vector output of the subordinate filters. Once an output is chosen, the state estimate and associated covariance matrix become the inputs for all filters on the subsequent step.

Using field data collected at the MIT Sailing pavilion, the filter system developed was shown to estimate current velocity and bias ratio using USBL data that was consistent with estimates calculated using higher accuracy LBL data. With the current velocity initialized at zero and the bias ratio initialized at 1, both values indicating no prior knowledge of the

parameters, the filter is able to converge on reasonable values during the approximately one hour run. The combination of estimating the bias ratio of the speed as well as the current velocity provides data to the end user that, in conventional approaches, requires the use of expensive equipment in terms of both acquisition cost and power consumption.

5.2 Recommendations for Further Research

While this thesis focused on low cost AUVs that are typically used by research teams in shallow water environments, the problem and the proposed solution also applies to other types of AUV such as autonomous underwater gliders (AUGs). AUG typically have a larger cost and size but, like small AUV, cannot maintain endurance with additions of sensors which increase power consumption or displacement. Unlike shallow water AUVs, AUGs encounter a wide variety of depths and stratification within the water column, resulting in a more complex current environment with vertical as well as horizontal structure. In order to accommodate this structure, the filter described in this thesis would have to be extended, perhaps by adding additional terms to the state vector.

As discussed in Chapters 2 and 3, not all of the statistical analysis methods for evaluating filter performance behaved as expected. While the NEES and NMEE demonstrated the effects of bias in simulation, the NIS remained consistent and did not show the effects of either the speed or the angle bias. Because the NIS is the only test of the three that can be used with experimental data and it did not perform as expected, methods other than statistical analysis were used to evaluate filter performance when processing field data. Over the course of many filter iterations, operator intuition into filter performance was built by observing patterns in characteristics such as the calculated current velocities to determine when the geometry of the problem would provide the most accurate filter output. For example, current velocity calculated on a steady track leg after a 180 degree turn was generally more accurate than the velocity calculated during a turn. Future applications would benefit from a summary statistic that provides a metric of filter performance without the heuristic process of developing operator intuition.

As demonstrated in Chapter 4, reprocessing the data with the bias ratio determined by the previous run resulted in the calculated value of the bias ratio continuing to rise, indicating that in order for the bias calculation process to be more robust, the run time of

the experiment should be longer to ensure the filter receives sufficient data to converge on a reasonable bias value.

Although a method for limiting the effects of outlier data was introduced in the filter construction, the system still demonstrated low robustness to inconsistent input data. Analysis of different tools to manage poor input data quality could significantly improve the output of the filter.

Bibliography

[1] Yaakov Bar-Shalom, X.-Rong Li, and Thia Kirubarajan. *Estimation with Applications to Tracking and Navigation*. John Wiley and Sons, Inc, New York, New York, 2001.

[2] Michael R. Benjamin, Henrik Schmidt, Paul M. Newman, and John J. Leonard. *Autonomy for Unmanned Marine Vehicles with MOOS-IvP*, pages 47–90. Springer New York, New York, NY, 2013.

[3] John L. Crassidis and John L. Junkins. *Optimal Estimation of Dynamic Systems*. CRC Press, Boca Raton, Florida, second edition, 2012.

[4] Seyed Fakoorian, Alireza Mohammadi, Vahid Azimi, and Dan Simon. Robust Kalman-Type Filter for Non-Gaussian Noise: Performance Analysis With Unknown Noise Covariances. *Journal of Dynamic Systems, Measurement, and Control*, 141(9), 05 2019. 091011.

[5] Ø. Hegrenaes and O. Hallingstad. Model-aided ins with sea current estimation for robust underwater navigation. *IEEE Journal of Oceanic Engineering*, 36(2):316–337, 2011.

[6] M. V. Jakuba, J. C. Kinsey, J. W. Partan, and S. E. Webster. Feasibility of low-power one-way travel-time inverted ultra-short baseline navigation. In *OCEANS 2015 - MTS/IEEE Washington*, pages 1–10, 2015.

[7] John J. Leonard and Alexander Bahr. *Autonomous Underwater Vehicle Navigation*, pages 341–358. Springer International Publishing, Cham, 2016.

[8] D. Lerro and Y. Bar-Shalom. Tracking with debiased consistent converted measurements versus ekf. *IEEE Transactions on Aerospace and Electronic Systems*, 29(3):1015–1022, 1993.

[9] Mae Seto Liam Paull, Sajad Saeedi and Howard Li. Auv navigation and localization - a review. *IEEE Journal of Oceanic Engineering*, 39(1):131–149,, 2014.

[10] N. R. Rypkema. *Underwater & Out of Sight: Towards Ubiquity in Underwater Robotics*. PhD dissertation, Massachusetts Institute of Technology and the Woods Hole Oceanographic Institution, Department of Electrical Engineering and Computer Science, September 2019.

[11] N. R. Rypkema, E. M. Fischell, and H. Schmidt. One-way travel-time inverted ultra-short baseline localization for low-cost autonomous underwater vehicles. In *2017 IEEE International Conference on Robotics and Automation (ICRA)*, pages 4920–4926, 2017.